Control of an Integrated Solar Thermal System based on Intelligent Iterative Learning for Hot Water Demand Prediction

by

Jacob Morrison

B.ASc. in Engineering Physics, Queen's University, 2017

A THESIS SUBMITTED IN PARTIAL FULFILLMENT OF THE REQUIREMENTS FOR THE DEGREE OF

MASTER OF APPLIED SCIENCE

in

The Faculty of Graduate and Postdoctoral Studies

(Mechanical Engineering)

THE UNIVERSITY OF BRITISH COLUMBIA

(Vancouver)

August 2020

The following individuals certify that they have read, and recommend to the Faculty of Graduate and Postdoctoral Studies for acceptance, the thesis entitled:

Control of an Integrated Solar Thermal System based on Intelligent Iterative Learning for Hot Water Demand Prediction

submitted by Jacob Morrison in partial fulfillment of the requirements for

the degree of Master of Applied Science

in Mechanical Engineering

Committee:

Supervisor Dr. Ryozo Nagamune, Mechanical Engineering

Examiner Dr. Clarence De Silva, Mechanical Engineering

Examiner Dr. Minkyun Noh, Mechanical Engineering

Abstract

In this thesis, an Iterative Learning (IL) approach to disturbance prediction that uses intelligent iteration grouping is proposed for Economic Model Predictive Control (EMPC), and applied to an Integrated Solar Thermal System (ISTS) in order to improve controller performance. An ISTS consists of a Solar Thermal Collector (STC) which collects energy from the sun, a Thermal Storage Tank (TST) which stores this energy for later use, and an auxiliary Heat Pump (HP) which acts as the actuator for the system, providing additional energy as required. The disturbance in the system is then the user hot water demand. In order to optimize the control performance of an ISTS with EMPC, it is important to be able to accurately predict this hot water demand before it happens. To solve this problem, a novel IL-based approach to disturbance prediction for EMPC is presented.

This approach involves separating long-term disturbance data, which in this case is user hot water demand, into a number of 24 hour iterations. These iterations are then further divided into groups using unsupervised learning based on the individual iteration profiles. Following the grouping of iterations, each iteration is given features such as the day of the week it occurs on, and a supervised learning classifier is trained to map from features to groups in order to predict the group of future iterations. Finally, IL is applied to learn patterns within each group iteratively and predict the actual hot water demand trajectory for future iterations.

A simulation of an ISTS using real world hot water demand data then demonstrates the effectiveness of the proposed approach to disturbance prediction, achieving higher performance EMPC than can be attained with existing disturbance prediction methods. Specifically, the EMPC implementation using the IL-based disturbance prediction algorithm is shown to prevent constraint violations within the ISTS more effectively than all other EMPC implementations while decreasing the average daily system cost by over 6%.

Lay Summary

A majority of the world currently relies on fossil fuels to meet energy demands. These resources are environmentally harmful and are nonrenewable, thus solar energy is becoming a more popular alternative. One application of solar energy is to provide hot water for household tasks. In this setting an additional heat source is often paired with the solar system to ensure that hot water demands can always be met. This added heat source is operated by a control system, which functions more efficiently if it knows how much hot water is required ahead of time. That is the main focus of this thesis, where a method for accurately predicting the future hot water demand for a household based on past hot water usage is presented. This accurate prediction improves the efficiency of the control system, thus reducing system costs and making the use of solar energy for heating applications more feasible.

Preface

This thesis is an original intellectual property of the author, Jacob Morrison. The thesis work was conducted under the supervision of Dr. Ryozo Nagamune.

Table of Contents

Appendix

List of Tables

List of Figures

Glossary

AB	Adaboost
ANN	Artificial Neural Network
ARANN	Hybrid approach that combines Autoregressive processes with Artificial Neural Networks
ARIMA	Autoregressive Integrated Moving Average Models
EMPC	Economic Model Predictive Control
GB	Gaussian Boosting
HP	Heat Pump
HWD	Hot Water Demand
HX	Heat eXchanger
IL	Iterative Learning
IP	Interior Point Optimization
ISTS	Integrated Solar Thermal System
KNN	K-Nearest Neighbors
MPC	Model Predictive Control
PID	Proportional-Integral-Derivative
PWM	Pulse Width Modulation

RF Random Forests

SQP Sequential Quadratic Programming

STC Solar Thermal Collector

SVM Support Vector Machines

TST Thermal Storage Tank

List of Symbols

A	Area $[m^2]$
A_{eff}	Solar thermal collector area $[m^2]$
A_ρ	Weighted averaging function
C_p	Specific heat capacity $[J/K]$
D	Number of past disturbance iterations to consider when calculating $\hat{W}$
D_α	Number of past disturbance iterations to consider when calculating α
E	Error in the primary prediction of a disturbance vector
$\mathcal{E}$	Set of error vectors
$\dot{E}_{hp}$	Power required to run the heat pump
$\dot{E}_{hp,f}$	Power required to run the heat pump at full heating capacity
$\dot{E}_{thermal}$	Rate of change of total energy in a system $[kJ/s]$
Err	Measurement of the total error in the final prediction of a number disturbance vectors
G_T	Solar intensity $[W/m^2]$
$\mathbb{J}$	Cost function for economic model predictive control
$\mathbb{J}_{\mathbb{CV}}$	Penalizes constraint violations in the cost function for economic model predictive control

$\mathbb{J}_{\mathbb{EC}}$	Penalizes economic cost in the cost function for economic model predictive control
$K_{\alpha\tau}$	Incident angle modifier for the solar thermal collector
m	Mass $[kg]$
$\dot{m}$	Mass flow rate $[kg/s]$
P_{hp}	Percentage of heating capacity used by the heat pump
$P_{\dot{E}_{hp}}$	Percentage of maximum power required by the heat pump
$\dot{Q}$	Heating capacity $[kJ/s]$
$\dot{Q}_{hp,f}$	Maximum heating capacity of the heat pump
$\dot{Q}_{in}$	Rate of change of energy entering a system from its surroundings $[kJ/s]$
$\dot{Q}_{in,E}$	Rate of change of energy entering a system $[kJ/s]$
$\dot{Q}_{out}$	Rate of change of energy leaving a system $[kJ/s]$
$\dot{Q}_{out,E}$	Rate of change of energy leaving a system to its surroundings $[kJ/s]$
$\mathcal{S}$	Arbitrary set of disturbance iteration vectors
T	Temperature $[K]$
$\dot{T}$	Rate of temperature change $[K/s]$
$\mathbf{T}$	Specific state space vector for a solar thermal system
T_{in}	Temperature entering a system $[K]$
T_{out}	Temperature leaving a system $[K]$
$\underline{\mathbf{T}}$	Component-wise lower boundary of the desired state vector range
$\bar{\mathbf{T}}$	Component-wise upper boundary of the desired state vector range

$\mathcal{T}_{est}$	Test set of disturbance iterations
u	Control input
U	Heat loss coefficient $[kJ/m^2Ks]$
$\mathcal{U}$	Control input range
V_{hp}	Compressor speed ratio of the heat pump
w	Disturbance in the form of hot water demand $[kg/s]$
W	Disturbance iteration vector
$\hat{W}$	Primary prediction of disturbance iteration vector
$\hat{\boldsymbol{W}}$	Final prediction of disturbance iteration vector
$\mathcal{W}$	Set of D disturbance iteration vectors of the same group
x	General state vector
α	Vector used in the equation for $\hat{\boldsymbol{W}}$
β	Steady shift operator
$\bar{\gamma}$	Soft upper constraint on the state vector
$\bar{\gamma}$	Soft lower constraint on the state vector
$\underline{\eta}$	Tuning parameter used in economic model predictive control
$\bar{\eta}$	Tuning parameter used in economic model predictive control
η_{stc}	Efficiency of the solar thermal collector
ρ	Weighting factor

Acknowledgements

First and foremost I would like to thank my supervisor Dr. Ryozo Nagamune for his unwavering guidance, support, and kindness throughout my studies here at the University of British Columbia.

I would also like to thank the Natural Sciences and Engineering Research Council of Canada's Collaborative Research and Development Grant, as well as Vladimir Grebenyuk and Ascent Systems Technologies for supporting this work financially.

Finally, I would like to thank my lab mates in the Control Engineering Laboratory for their incredible camaraderie and insight.

Dedication

I would like to dedicate this thesis to my family and friends, for without them none of this would have been possible.

Chapter 1

Introduction

A majority of the world currently relies on fossil fuels to meet energy demands. These resources are harmful to the environment and do not replenish themselves, causing energy prices to rise as they become more and more scarce [1]. One abundantly available renewable alternative is the sun, which provides the earth with more raw energy in one hour than the human population consumes in an entire year [2]. When it comes to solar energy, solar thermal systems are the most efficient option and are typically used for heating applications as opposed to electricity production. While heating is not the only energy requirement for humans, it represents a crucial area of need. This need is particularly strong in northern countries such as Canada, where hot water accounts for approximately 25% of domestic energy consumption [3].

1.1 Solar Thermal Systems

The idea of harnessing the sun's energy for heating applications has been around for some time. In fact, the origin of solar thermal systems as they are known today can be traced back to patents from the early 1900's [4]. These systems are employed all over the world, providing renewable heat energy to numerous countries. This technology is also used in a wide range of applications, from large solar thermal power plants which provide heat to large factories, to small residential systems that provide hot water to individual households [5–7]. Some examples of solar thermal systems in use can be seen in Fig. 1.1. This thesis focuses specifically on domestic solar thermal systems.

Two main components form the backbone of modern residential solar thermal systems. These are the Solar Thermal Collector (STC) which absorbs the thermal energy from the sun, and the Thermal Storage Tank (TST) which stores this energy for future use, acting as a sort of battery for the system. Most domestic solar thermal systems also feature an auxiliary heat source to ensure hot water demands can always be met. The combination

(a) Example of a large solar thermal power plant (https://www.sciencealert.com)

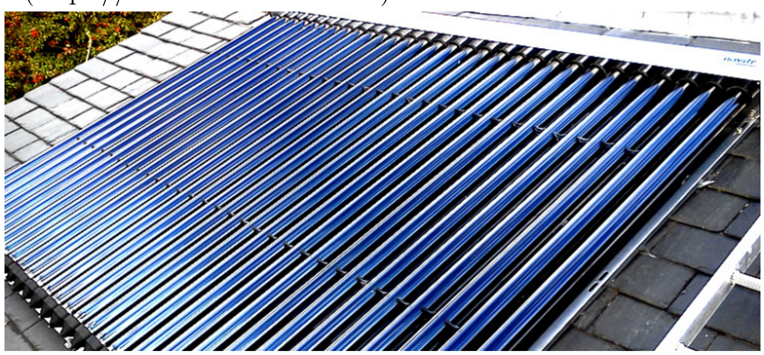

(b) Example of a small residential solar thermal setup (https://www.thegreenage.co.uk)

Figure 1.1: Two examples showing the wide variation in scale of solar thermal systems

of this external source with an STC is called an Integrated Solar Thermal System (ISTS), which is the primary subject of this thesis.

1.2 Problem Statement

In order to truly realize the potential in harnessing the sun's energy, the systems in place to harness it must provide clear incentives relative to classical energy production methods, beyond just that of decreased environmental impact. In residential settings, solar thermal systems are not nearly as prevalent as other more traditional methods for hot water heating such as gas and electric. The main reason for this is the high upfront cost to implement a solar thermal system, coupled with limited future returns. These limitations in returns are due to inefficiencies in current implementations of ISTSs for domestic applications. With this in mind, by improving the performance of ISTSs, their wide spread use becomes a lot more viable.

The goal of this research is to improve the performance of domestic ISTSs from a control engineering perspective. This means decreasing the operating costs of the system while simultaneously improving the ISTS' adherence to hot water temperature constraints relative to existing control methods. This will be accomplished by accurately predicting future Hot Water Demand (HWD) in a given household, and incorporating this prediction into a modern control algorithm so as to increase the algorithms effectiveness in the context of this domestic solar thermal application.

1.3 Control Review of an ISTS

When it comes to controlling an ISTS, it is important to maximize efficiency by using the auxiliary heat source intelligently. Past research into this application has found Economic Model Predictive Control (EMPC) to be the most effective control algorithm as it can be optimized while accounting for case specific factors such as input constraints. Halvaard et al. used simple linear EMPC for a smart solar tank to control the temperature of a house, showing that EMPC led to a decrease of up to 25% in annual electrical costs compared to a simple on/off controller, provided the prediction horizon was sufficiently long [8]. Godina et al. further highlighted the benefits of EMPC by comparing its performance with on/off and Proportional-Integral-Derivative (PID) controllers for domestic energy management. They found that the use of EMPC saved consumers approximately 9.2% in energy consumption costs [9]. Weeratunge et al. then provided more insight by using EMPC to reduce the operational costs of a solar assisted heat pump system compared to conventional control methods, achieving a 7.8% cost reduction [10].

1.3.1 Economic Model Predictive Control

Model Predictive Control (MPC) is a predictive feedback control methodology that optimizes the control input of a process through the use of a process model while satisfying system specific constraints [11]. EMPC builds on MPC by incorporating the economic cost of the process into the cost function to be optimized. As a result, EMPC is able to combine economic optimization with optimal system performance, which has led to a rapid increase in its popularity in the process control industry [12]. Numerous studies have examined the impact of EMPC, demonstrating its benefits across various applications from chemical process control [13, 14] to building energy control [15, 16]. The range of applications where EMPC is effective also includes solar thermal systems, and EMPC represents the base control algorithm used in this research.

1.3.2 Shortcomings

An issue with the majority of research to date into EMPC for solar thermal and general energy saving applications, however, is the lack of consideration for the impact of different user load scenarios. In relation to domestic solar thermal systems used for heating water, most works assume a constant daily HWD profile for simplicity [17], whereas in reality user load can vary drastically, both day-to-day within a household and between different households [18]. This is an area of concern as EMPC algorithms tend to behave poorly when system output predictions are inaccurate, which would be the case with any model that assumes a single load trajectory. EMPC algorithms have even been shown to perform worse than a classical PID controller in the presence of disturbance prediction error, both in terms of constraint violation and economic cost [19].

To overcome this challenge, a number of disturbance prediction methods have been proposed, including time-series methods such as Autoregressive Integrated Moving Average Models (ARIMA) [20–22], and hybrid approaches that combine autoregressive processes with artificial neural networks (ARANN) [23, 24]. While useful in certain settings, these methods require constant online updates, which can be quite taxing computationally for many process control problems that already incorporate online optimization for EMPC [25, 26]. Further, these types of time-series methods tend to perform poorly when it comes to long-term prediction. Such poor disturbance prediction is an issue when it comes to implementing EMPC, as this control scheme requires accurate prediction of the state trajectory over the entire control horizon [27].

1.4 Research Outline

One aspect of many control problems that can be exploited in order to provide more accurate prediction is a cyclic nature to the disturbance pattern. Humans are creatures of habit who tend to repeat similar daily routines. As a result, any control problem that features human load usage will tend to have a repetitive disturbance. This involves the control of any process dealing with daily human consumption from electricity use to internet activity levels to any type of heating or cooling application across commercial, residential, and industrial settings [28–31]. Of course, this also includes domestic ISTSs for heating water. While different households use different amounts of hot water and this usage can vary day-to-day, individual households often follow repetitive load profile patterns [32, 33]. With this repetitive property in mind, an effective approach for HWD prediction in the ISTS application is to utilize Iterative Learning (IL) techniques to take advantage of the repetitive nature of domestic hot water usage.

IL is based on the idea that the performance of a system completing a repetitive task can be improved by learning from past iterations of the task [34]. To date some attempts to combine IL with MPC have been undertaken in literature. These efforts have mainly focused on using IL to update the terminal constraints in the MPC algorithm [35], or to improve controller performance in batch processes by iteratively updating the model parameters or state estimation [36, 37]. Contrarily, the idea presented in this research is to employ the IL framework to predict future disturbances, allowing for more effective control.

In order to maximize the disturbance prediction performance of IL, it is beneficial to sort disturbance iterations into groups. When discussing domestic hot water consumption, the period of repetition is 24 hours. The consumption pattern over each of these iterations adheres to some cyclic pattern, but will not be constant and can fluctuate drastically from one iteration to the next [17]. With these fluctuations in mind, by grouping similar iteration types together before applying IL, the patterns of each specific group can be learned separately, allowing for more accurate prediction than could be achieved by simply using IL to learn the general pattern of all iterations combined.

When it comes to grouping disturbance iterations for the purpose of aiding in IL-based prediction, however, it is also necessary to predict which group future iterations will likely belong to. This means that the grouping process as a whole involves both the clustering and classification of disturbance iterations. There are a number of ways to tackle these tasks ranging from simple naive methods, such as grouping and classifying iterations based on a single measurable feature, to more complex methods, such as incorporating machine learning techniques. This research will explore the intelligent grouping and classifying of iterations using both supervised and unsupervised machine learning methods, and present this approach along with the IL idea discussed above.

The main contribution of this thesis is to propose a novel IL-based disturbance prediction algorithm that works to improve EMPC performance to a level that cannot be achieved with existing disturbance prediction methods. This algorithm iteratively analyzes grouped disturbance iterations, recognizes patterns within each group, and uses these patterns to make disturbance predictions for future iterations. In order to improve the functionality of the algorithm, a machine learning based procedure to group the disturbance iterations intelligently is also proposed as a further contribution of this research.

1.5 Thesis Organization

In order to convey the contributions described above in Section 1.4, this thesis is organized as follows. In Chapter 2, a description of the specific ISTS considered in this research is given, and a state space model for the system is detailed. The control objectives are then explained in Chapter 3 and the EMPC strategy is designed. The IL algorithm for disturbance prediction is then presented as a means to improve the performance of the designed EMPC in Chapter 4. Next, the grouping aspect of the IL algorithm is further explored in Chapter 5, and a procedural approach to iteration clustering and classification using machine learning is described. A system simulation using real domestic hot water consumption data demonstrates the efficiency of the proposed IL-based disturbance prediction approach to EMPC in Chapter 6. Finally, the research outcome is summarized in Chapter 7 and potential areas for future work are discussed.

Chapter 2

System Description

In this chapter, the ISTS considered in this research is introduced and a discrete-time nonlinear state space model for the ISTS is described.

2.1 Integrated Solar Thermal System

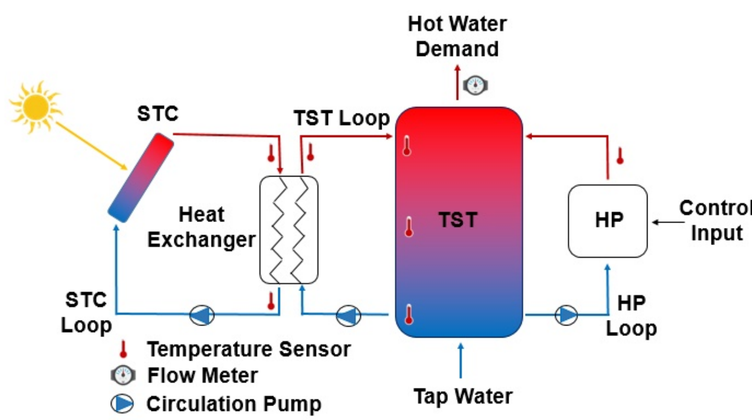

Figure 2.1: Integrated solar thermal system configuration

The ISTS in question features an STC, a TST, and an auxiliary heat source in the form of an electric Heat Pump (HP). All components are set up in a parallel fashion as seen in Fig. 2.1. The system has three loops, each containing a pump operating at a constant speed to circulate the fluid inside. In the STC loop the working fluid is glycol, while in the other loops it is water. A Heat eXchanger (HX) is used to transfer heat from the STC loop to the TST loop. The HP loop then supplies further heat to the TST as needed. The control input for the system deals with actuating the compressor speed ratio of the HP to select the amount of auxiliary heat added to the system and will be described in more detail later on. Finally, the user HWD is taken from the top of the TST and is replaced by relatively cold tap water at the bottom. The system also features numerous temperature sensors to measure the temperature of the working fluid at different points throughout the configuration, as well as a flow meter that measures the HWD.

2.2 State Space Model

Consider a general discrete-time nonlinear state space model:

$$x_{k+1} = f(x_k, u_k, w_k), \tag{2.1}$$

where $x_k \in \mathbb{R}^n$ is the state vector at time k, $u_k \in \mathbb{R}^m$ is the control input at time k, $w_k \in \mathbb{R}$ is the disturbance vector at time k, and f is a nonlinear function with respect to these vectors.

For the specific model describing the ISTS seen in Fig. 2.1, this discrete-time nonlinear state space model takes the following form:

$$\mathbf{T}_{k+1} = f(\mathbf{T}_k, u_k, w_k) \tag{2.2}$$

Here $\mathbf{T} \in \mathbb{R}^n$ is the state vector consisting of the fluid temperatures at n different locations in the ISTS, measured with n temperature sensors placed throughout the system. This n state setup serves as a lumped approximation to the real system. Additionally, $u \in \mathbb{R}$ is the compressor speed ratio of the HP and $w \in \mathbb{R}$ is the user HWD ($\dot{m}_{hwd}$) [$\frac{Kg}{s}$]. Lastly, the output (y) of the model is the temperature at the top layer of the TST.

The details of the nonlinear function $f(\mathbf{T}_k, u_k, w_k)$ describing the rate of temperature change in the various locations of the ISTS are then detailed throughout the rest of this section. Note that the presented equations describe a continuous-time system, but this system was discretized for use in EMPC, as described in Chapter 3. A 7-state version of the general state space model in continuous-time can be seen in closed form in the Appendix. In the 7-state case the locations of the seven fluid temperatures comprising the state vector are denoted by the temperature sensors in Fig. 2.1.

2.2.1 Conservation of Energy

When it comes to modeling a thermal system, the fundamental equation to consider is the conservation of energy principle:

$$\dot{Q}_{in} - \dot{Q}_{out} = \dot{E}_{thermal}, \tag{2.3}$$

where $\dot{Q}_{in}$ [$\frac{kJ}{s}$] and $\dot{Q}_{out}$ [$\frac{kJ}{s}$] are rates of changes of the total energy entering the system and total energy leaving the system, respectively. $\dot{E}_{thermal}$ [$\frac{kJ}{s}$]

is then the rate of change of the total energy of the system. This term can then be written as

$$\dot{E}_{thermal} = mC_p\dot{T}, \tag{2.4}$$

with $m[kg]$ being the mass of the fluid in the system, C_p $[\frac{J}{K}]$ being the specific heat capacity of the fluid, and $\dot{T}$ $[\frac{K}{s}]$ being the time rate of change of the fluid temperature. Additionally, $\dot{Q}_{in}$ and $\dot{Q}_{out}$ can be further broken down as

$$\dot{Q}_{in} = \dot{m}C_pT_{in} + \dot{Q}_{in,E}, \tag{2.5}$$

$$\dot{Q}_{out} = \dot{m}C_pT_{out} + \dot{Q}_{out,E}, \tag{2.6}$$

where $\dot{m}$ $[\frac{kg}{s}]$ is the mass flow rate of the fluid and T_{in} $[K]$ and T_{out} $[K]$ are the fluid temperatures at the inlet and outlet of the system, respectively. Here the first term in each equation represents the rate of energy added to or taken from the system by moving fluid, and the second term in each represents the rate of energy being added to ($\dot{Q}_{in,E}$ $[\frac{kJ}{s}]$) or removed from ($\dot{Q}_{out,E}$ $[\frac{kJ}{s}]$) the system by its surroundings.

In the following subsection, this idea of the conservation of energy is explored for each of the individual components of the ISTS.

2.2.2 Component Modeling

To begin, components that can be modeled as static systems are examined. These are the STC and the HP.

Solar Thermal Collector

Energy generated by the STC can be described as follows:

$$\dot{Q}_{stc} = A_{eff}G_TK_{\alpha\tau}\eta_{stc}. \tag{2.7}$$

Here A_{eff} $[m^2]$ is the area of the STC normal to the solar radiation, G_T $[\frac{W}{m^2}]$ is the solar intensity which is based on the relative position of the sun and the STC, $K_{\alpha\tau}$ is the incident angle modifier, and η_{stc} is the efficiency of the STC as provided by the manufacturer of the specific STC being used. Note that the specific method for calculating A_{eff}, G_T, and $K_{\alpha\tau}$ is given in [38]. The temperature of the fluid leaving the STC is then computed as

$$T_{out,stc} = T_{in,stc} + \frac{\dot{Q}_{stc}}{\dot{m}_{stc}C_{p,stc}}. \tag{2.8}$$

Heat Pump

Similar to the STC, the temperature of the fluid exiting the HP can be found using:

$$T_{out,hp} = T_{in,hp} + \frac{\dot{Q}_{hp}}{\dot{m}_{hp} C_{p,hp}}, \tag{2.9}$$

where $\dot{Q}_{hp}$ is the energy supplied by the HP. In this case $\dot{Q}_{hp}$ is written as

$$\dot{Q}_{hp} = \dot{Q}_{hp,f} P_{hp}, \tag{2.10}$$

where $\dot{Q}_{hp,f}$ is the maximum heating capacity of the HP as given by the manufacturer and P_{hp} is the percentage of the heating capacity used based on the input compressor speed ratio of the HP. This percentage can be calculated based on work done in [38] using:

$$P_{hp} = -0.3498 V_{hp}^2 + 1.35 V_{hp}, \tag{2.11}$$

where V_{hp} is the compressor speed ratio of the HP and is equivalent to u in (2.2).

Note that the nature of the heat pump and the compressor speed ratio will be discussed in further detail in Chapter 3. For now the focus shifts to dynamic components of the ISTS.

Heat Exchanger

In the HX, hot glycol from the STC loop flows through a cylindrical coil in one direction, while relatively cold water from the TST loop flows through a shell surrounding the coil in the other direction. As a result of the close proximity of these two fluids, heat is transferred from the glycol to the water. In addition to the heat gained from the glycol, the water in the shell may also lose some heat to the surrounding air. The resulting equations for $\dot{Q}_{in,E}$ and $\dot{Q}_{out,E}$ within each control volume inside the HX are:

$$\dot{Q}_{in,E} = U_{coil} A_{coil} (T_{glycol} - T_{water}), \tag{2.12}$$

$$\dot{Q}_{out,E} = U_{shell} A_{shell} (T_{water} - T_{amb}). \tag{2.13}$$

Here $U_{coil}[\frac{kJ}{m^2 Ks}]$ and $U_{shell}[\frac{kJ}{m^2 Ks}]$ are respectively the heat loss coefficients between the glycol and the water, and between the water and the air. These can be determined based on the specifics of the HX being used along with the heat transfer coefficients between glycol and water and between water and air. Further, $A_{coil}[m^2]$ is the area of contact between the coil and the shell within each control volume, $A_{shell}[m^2]$ is the area of contact between the shell and the surrounding air within each control volume, $T_{glycol}[K]$ is the glycol temperature inside the coil within each control volume, $T_{water}[K]$ is the water temperature inside the shell within each control volume, and $T_{amb}[K]$ is the ambient air temperature.

Thermal Storage Tank

The TST in this ISTS is a cylindrical tank with a vertical orientation that is filled with water. For modeling purposes the volume of the TST is broken into a number of layers where it is assumed that the temperature of the water within each layer is uniform, and that the temperature gradually decreases from the top layer to the bottom layer. It is further assumed that the flow rate of the tap water entering the bottom of the TST is equal to the HWD such that the volume in the TST remains constant, and that each layer in the TST simultaneously experiences three separate flows. These flows consist of the flow through the TST loop ($\dot{m}_{tst}$), the flow through the HP loop ($\dot{m}_{hp}$), and the HWD ($\dot{m}_{hwd}$). The resulting energy balance for convective heat transfer to and from the water in the j^{th} level of the TST due to these flows is then given as

$$\dot{Q}_{outlet} - \dot{Q}_{inlet} = C_p(\dot{m}_{tst} + \dot{m}_{hp})(T_j - T_{j+1}) + C_p\dot{m}_{hwd}(T_{j-1} - T_j). \quad (2.14)$$

Here T_j of course represents the temperature of the water in the j^{th} level of the TST. The heat loss from level j to the surrounding air is then given as

$$\dot{Q}_{out,E} = U_{tst}A_{j,tst}(T_j - T_{amb}), \quad (2.15)$$

where again $U_{tst}[\frac{kJ}{m^2Ks}]$ is the heat loss coefficients between the water in level j of the TST and the surrounding air, and $A_{j,tst}[m^2]$ is the area of contact between the j^{th} level of the TST and the surrounding air. Note that conductive heat transfer between the various fluid levels within the TST is assumed to be negligible and is thus ignored.

Pipes

In this sort of ISTS the pipes lead to negligible heat loss relative to other heat loss in the system, as was shown by Rostam et al. in [39]. This means that fluid temperature is assumed to be constant as fluid flows through the pipes, and the effect of the pipes can be ignored in developing the state space model.

Chapter 3

Controller Design

In this chapter, the control objectives for the ISTS are stated and the base EMPC set up for use in realizing these objectives is defined.

3.1 Control Objective

The control objectives for the ISTS are as follows:

(O1) Maintain the top layer temperature in the TST within a desired temperature range at all times by regulating the compressor speed ratio of the HP.

(O2) Minimize HP operating costs while completing (O1).

The main challenge in achieving these objectives is the varying nature of hot water demand. The ideal controller must be able to efficiently perform the control task for households featuring a unique load pattern that changes over time.

3.2 Economic Model Predictive Control

For the ISTS, an EMPC problem with a prediction horizon of N can be formulated as follows [40]:

$$\begin{aligned} \min_{\substack{\{u_{k+j|k} \in \mathcal{U}\}_{j=1}^{N}, \\ \{(\underline{\gamma}_j, \bar{\gamma}_j)\}_{j=1}^{N}}} \quad & \sum_{j=1}^{N} \mathbb{J}(\mathbf{T}_{k+j|k}, u_{k+j|k}, \underline{\gamma}_j, \bar{\gamma}_j, k), \\ \text{s.t.} & \begin{cases} \mathbf{T}_{k+j+1|k} = f(\mathbf{T}_{k+j|k}, u_{k+j|k}, \hat{w}_{k+j|k}), \\ \underline{\mathbf{T}} - \underline{\gamma}_j \leq \mathbf{T}_{k+j|k} \leq \bar{\mathbf{T}} + \bar{\gamma}_j, j = 1, \ldots, N. \end{cases} \end{aligned} \tag{3.1}$$

Here $\underline{\mathbf{T}} \in \mathbb{R}^n$ and $\bar{\mathbf{T}} \in \mathbb{R}^n$ respectively represent the component-wise lower and upper boundaries of the desired range of the state vector, and the notation $v_{k+j|k}$ indicates the value of a vector v at time $k+j$ when calculated at time k. Further, the control input for the system is constrained to $\mathcal{U} := [0, 1]$ with zero relating to the HP being turned off and one relating to the HP functioning at full heating capacity. Lastly, to maintain the state vector within the desired range while allowing slight violations to avoid an infeasible optimization problem, soft constraints are applied with the non negative slack variables $\bar{\gamma}_j \in \mathbb{R}^n$ and $\underline{\gamma}_j \in \mathbb{R}^n$. Note that (3.1) can be solved using various non-convex optimization methods such as the Interior Point Optimization (IP) method or Sequential Quadratic Programming (SQP) [41, 42].

The cost function $\mathbb{J}$ in (3.1) consists of two terms:

$$\mathbb{J}(x, u, \underline{\gamma}, \bar{\gamma}, k) := \mathbb{J}_{\mathrm{EC}}(x, u, k) + \mathbb{J}_{\mathrm{CV}}(\underline{\gamma}, \bar{\gamma}). \tag{3.2}$$

The first term $\mathbb{J}_{\mathrm{EC}}$ represents the economic cost of operating the system while the second term $\mathbb{J}_{\mathrm{CV}}$ penalizes state constraint violations. The second term is detailed further as

$$\mathbb{J}_{CV}(\underline{\gamma}, \bar{\gamma}) := \underline{\eta}\|\underline{\gamma}\|^2 + \bar{\eta}\|\bar{\gamma}\|^2, \tag{3.3}$$

where the positive scalar constants $\underline{\eta}$ and $\bar{\eta}$ can be tuned to increase or decrease the controller's emphasis on preventing constraint violations.

Looking again at (3.1), $\hat{w}_{k+j|k}$ indicates the disturbance prediction at time k for time $k + j$. It is this distrubance prediction that is the main focus of this research. In the past, research into EMPC has considered two common approaches to deal with this disturbance prediction. The first is to simply use the average disturbance profile for prediction [43, 44]. The issue here is that the prediction will tend to be inaccurate in many cases, leading to poor controller performance. The second common approach is a robust approach that uses the worst possible disturbance for prediction [45, 46]. This method may lead the controller to be overly conservative, resulting in unnecessarily high economic cost to the system.

3.3 Actuator Limitations

As described in the previous chapter, the input u for the ISTS is the compressor speed ratio of the HP. Theoretically it makes sense that a HP could contain a variable speed compressor and so any input between 0 and 1 would be possible. In reality though, the vast majority of commercially available HPs are two-stage or three-stage. A two-stage HP is such that its only operational level is at full heating capacity which corresponds to input values of either $u = 0$ or $u = 1$, while a three-stage HP can operate at input values of $u = 0$, $u = 0.5$, or $u = 1$. As a result, the conventional EMPC approach described in the previous section is not feasible here.

3.3.1 Possible Approaches

In order to implement EMPC despite the compressor speed limitations associated with most HPs, there are two options. The first is to implement a variation of EMPC that optimizes a set of discrete inputs over the control horizon. Depending on the HP available, this could be done using only inputs of 0 and 1 or with inputs of 0, 0.5. and 1. An example of the formulation of this sort of EMPC using on/off inputs can be found in [47]. The issue with this approach is that there will inevitably be degradation of the control performance from both a constraint violation perspective and an economic cost perspective relative to that of normal EMPC paired with a variable speed HP. If at any point the optimal control input for the next time step is a value outside of the set of possible discrete input values, then the performance of the discrete EMPC approach will fall short of the normal EMPC approach. Additionally, the new discrete EMPC problem becomes much harder to optimize than the problem presented in (3.1).

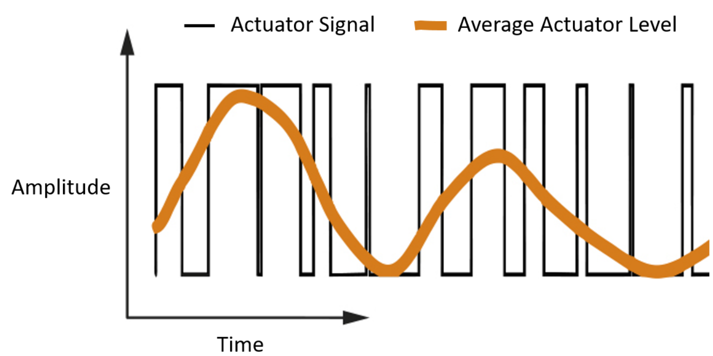

Figure 3.1: Pulse width modulation example

The second option is to utilize Pulse Width Modulation (PWM), which allows two-stage and three-stage HPs to function as variable speed HPs as far as control algorithms are concerned [48]. The way PWM works for an on/off actuator is to turn the actuator fully on for a portion of each time step so as to replicate the effect of the actuator acting at some level less than 100% for the entire time step. An example of this is displayed in Fig. 3.1, where the black line represents the actual actuator signal while the brown line represents the average actuator level over each time step. This process can also be adapted to a three-stage actuator by pulsing the actuator at 50% to achieve output levels below 50% and pulsing the actuator between 100%

and 50% to achieve output levels above 50%. From an EMPC perspective, PWM allows the algorithm to function as intended, determining the optimal control input from a continuous set. In the ISTS environment, this optimal input is then implemented by pulsing a two-stage or three-stage heat pump for the correct portion of the time step as opposed to simply setting the compressor speed ratio to the optimal input for the whole time step.

The clear benefit of the PWM approach relative to the discrete EMPC approach is that the former will perform identically to a true variable speed HP from a constraint violation perspective. This is true for both two-stage and three-stage HPs so long as the frequency of actuator action comes in at approximately one actuation or less every 5 minutes. This limit is in place so as to prevent damage to the pump [49]. As a result, the time step for control action in the ISTS should be set no lower than 10 minutes, which is very reasonable considering the relatively slow nature of thermal systems.

While the PWM approach allows an ISTS with a two-stage or three-stage HP to function as if it had a variable speed HP as far as constraint violations are concerned, it will lead to increased costs due to the nature of heat pump power and energy curves. These costs are analyzed in the following subsection.

3.3.2 Pulse Width Modulation Cost Analysis

In order to compare the cost of a PWM approach with a two-stage HP and with a three-stage HP to that of a variable speed HP, it is first necessary to determine how to implement PWM. Looking to (2.11) it can be seen that $P_{hp}(1) = 1$. This implies that for implementing the two-stage case it is simply a matter plugging the desired compressor speed ratio into (2.11), obtaining an operating percentage, and turning the two-stage HP on for that same percentage of the time step. The three-stage case requires slightly more work but can also be determined from (2.11).

The cost of operating the HP can then be calculated by multiplying the amount of electrical power needed by the cost of electricity. The amount of power needed is actually calculated in a very similar manner to the heating capacity calculation in (2.10), with the power calculation given as

$$\dot{E}_{hp} = \dot{E}_{hp,f} P_{\dot{E}_{hp}}. \tag{3.4}$$

Here $\dot{E}_{hp}$ is the power required to run the HP, $\dot{E}_{hp,f}$ is the power required to run the HP at full heating capacity, and $P_{\dot{E}_{hp}}$ is the percentage of that full power actually needed. $P_{\dot{E}_{hp}}$ is based on the compressor speed ratio and can be found using the following equation based on work completed in [38]:

$$P_{\dot{E}_{hp}} = 0.2597V_{hp}^2 + 0.7448V_{hp}. \tag{3.5}$$

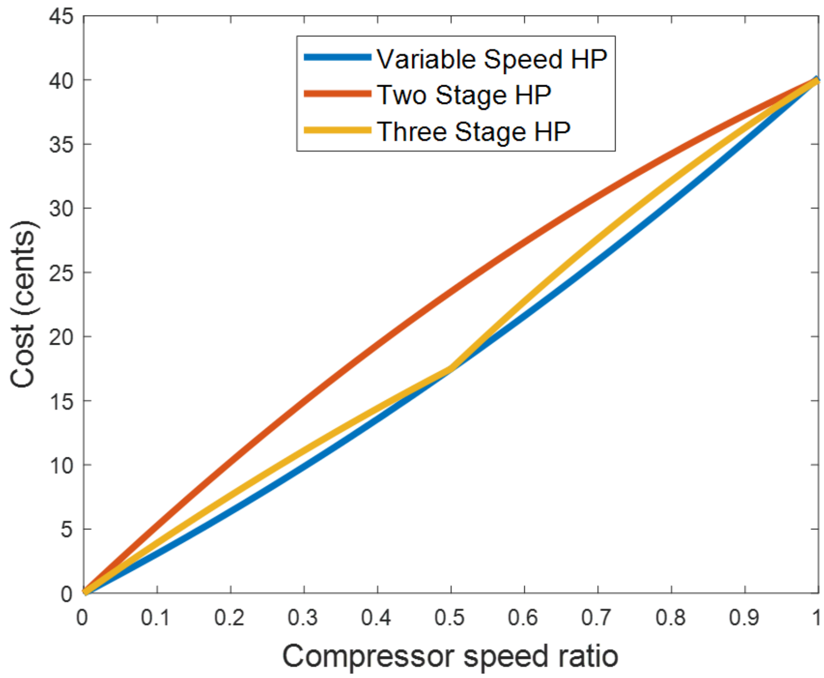

Figure 3.2: Cost comparison between a two-stage HP, a three-stage HP, and a variable speed HP at various compressor speed ratios

The actual cost and heating capacity of a HP will depend on the specific HP being used. Therefore, some assumptions must be made in order to compare the cost of a two-stage HP with PWM, the cost of a three-stage HP with PWM, and the cost of a variable speed HP in a general sense. Firstly, it is assumed that all HPs are identical in terms of their maximum heating capacity, and this value is assumed to be 8 kW. The cost of electricity is then taken as 10 cents per kWh. Based on these assumptions, a cost comparison of the three HP options can be seen in Fig. 3.2. In the figure, the blue curve represents the cost to run the variable speed HP for an hour at the various compressor speed ratios. The red and yellow curves then represent the minimum cost to supply the same amount of heat energy with a two-stage HP and a three-stage HP, respectively. It is clear in the figure that, due to the discrepancy between the power and the heat capacity curves, the PWM approach costs more to supply the same amount of heat energy. That being said, the three-stage HP is much more cost effective than the two-stage HP, and offers very comparable costs to that of the variable speed HP.

To conclude, three-stage HPs are available for purchase and, when incorporating PWM, are able to perform quite similarly to variable speed HPs. Further, the PWM approach allows EMPC to be implemented as described by (3.1).

In the next chapter, an effective approach to determining $\hat{w}_{k+j|k}$ in (3.1) based on the concept of IL is proposed so as to improve the performance of the ISTS.

Chapter 4

Iterative Learning for Disturbance Prediction

In order to achieve the control objectives defined by (3.2), a controller structure is proposed in Section 4.1, followed by a description of the disturbance prediction problem to be solved in Section 4.2 and an explanation of a novel solution to this problem in the form of an IL method for disturbance prediction in Section 4.3. The memory requirements of the proposed IL method are then defined in Section 4.4 and a theorem supporting the validity of the proposed IL approach is provided in Section 4.5. Note that, while the disturbance in this research is the HWD of the ISTS, this chapter is written so as to describe the IL approach to disturbance prediction in general.

4.1 Control Framework

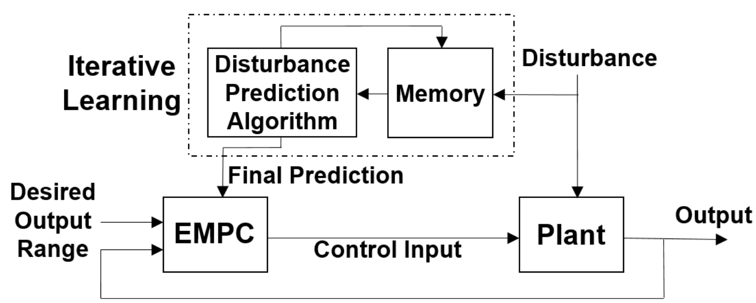

Figure 4.1: Control framework of proposed method

In typical IL control, the error in a system's output relative to a reference trajectory is used to adjust the input for the next iteration [34]. In contrast, this research uses disturbance information from past iterations along with the error in past predictions to make disturbance predictions for the next iteration. The block diagram for the control framework is depicted in Fig. 4.1.

In this framework, previous disturbance information is fed into the IL portion (dash-dotted rectangle in Fig. 4.1) of the controller, which outputs an updated disturbance trajectory prediction after each iteration for use in the EMPC system model. Note that, in addition to the prediction algorithm, the IL portion of the disturbance predictor also contains a memory component to store past information for use in future predictions. The specifics of the IL prediction process are detailed further in Section 4.3.

4.2 Disturbance Trajectory Prediction Problem

In order to formulate a disturbance trajectory prediction problem, some notation is first introduced:

$$W := \left[\; w_1, \quad w_2, \quad \ldots, \quad w_{k_f} \right]. \tag{4.1}$$

Here W is a disturbance iteration that contains k_f discrete disturbance values representing its disturbance trajectory. Now consider a series of M disturbance iterations:

$$W_1, W_2, \ldots, W_M, \tag{4.2}$$

where the subscript of W denotes the iteration number and $W_i \in \mathbb{R}^{k_f}$, $i = 1, 2, \ldots, M$.

Iterations can also be grouped with the help of a grouping strategy. The specific intelligent iteration grouping strategy used in this paper is detailed in Chapter 5. Based on the chosen grouping strategy, if a disturbance iteration W_i belongs to group g_i then this grouping will be indicated with the superscript as $W_i^{(g_i)}$.

As an example, let us assume a six-day disturbance signal that exhibits one distinct pattern on weekdays and another on weekends. This signal can be divided into six iterations W_i, $i = 1, \ldots, 6$. If it is assumed that the first iteration occurs on a Wednesday and iterations are naively grouped based on whether they fall on a weekday ($g = 1$) or a weekend ($g = 2$), then the six iterations can be denoted with grouping information as

$$W_1^{(1)}, W_2^{(1)}, W_3^{(1)}, W_4^{(2)}, W_5^{(2)}, W_6^{(1)}. \tag{4.3}$$

A possible sequence of disturbance iterations for such a system, along with their groupings, are displayed in Fig. 4.2. Here it is clear that the weekdays and the weekend days have different patterns, with the peak value in the morning and in the evening respectively.

With the notation described above, the disturbance profile prediction problem is then formulated as follows.

Problem 1. *It is assumed that the past M disturbance iterations are known, and that they have been grouped into G separate groups:*

$$W_i^{(g_i)},\ g_i \in \{1, \ldots, G\},\ i = 1, \ldots, M. \tag{4.4}$$

It is also assumed that the group g_{M+1} of iteration $M+1$ is known, even though the future disturbance trajectory W_{M+1} is not. Under these assumptions the disturbance prediction problem is to obtain a prediction for the next iteration $W_{M+1}^{(g_{M+1})}$ denoted by $\hat{\boldsymbol{W}}_{M+1}^{(g_{M+1})}$.

When related directly to the previous example, Problem 1 is to predict the disturbance trajectory for the seventh iteration based on the disturbances from the previous six iterations.

4.3 Disturbance Trajectory Prediction Algorithm

In this subsection the proposed disturbance trajectory prediction algorithm will be presented mathematically. The prediction algorithm actually consists of two sub-algorithms, which are denoted the primary prediction algorithm and the final prediction algorithm. As a compliment to the mathematical descriptions of these two algorithms, further explanations and examples will be given in Section 4.3.1 and Section 4.3.2 for the primary prediction and final prediction algorithms, respectively.

To begin, let us consider general set of K vectors

$$\mathcal{V}_K := \{v_1, v_2, \ldots, v_K\}. \tag{4.5}$$

A weighted averaging function for this general set of vectors can then be defined as

$$A_\rho \{\mathcal{V}_K\} := \frac{1}{\sum_{d=1}^{K} \rho_d} \sum_{d=1}^{K} \rho_d v_{K+1-d}, \tag{4.6}$$

with $\rho \in \mathbb{R}_+^K$ being a given weighting factor selected by the user on a case by case basis. Note that in the case where $\rho = \vec{1}$ then the averaging function will simply be denoted as A.

Next, a set of the previous D disturbance iteration vectors belonging to the same group g and occurring on or before iteration M can be defined as $\mathcal{W}_{M,D}^{(g)}$. Using the example from Section 4.2 again, the set of the last 3 iteration vectors in group $g = 1$ occurring on or before iteration 6 is defined as:

$$\mathcal{W}_{6,3}^{(1)} := \left\{W_6^{(1)}, W_3^{(1)}, W_2^{(1)}\right\}, \tag{4.7}$$

while the set of the last 2 iterations in group $g = 2$ is:

$$\mathcal{W}_{6,2}^{(2)} := \left\{ W_5^{(2)}, W_4^{(2)} \right\}, \tag{4.8}$$

With this notation in place, the following iterative algorithm for the primary disturbance trajectory prediction is proposed:

$$\hat{W}_{M+1}^{(g_{M+1})} = A_\rho \left\{ \mathcal{W}_{M,D}^{(g_{M+1})} \right\} \tag{4.9}$$

In this algorithm, the primary disturbance trajectory prediction for iteration $M+1$ is taken as a weighted average of the disturbance trajectories for the past D iterations belonging to group g_{M+1}. Note that $\hat{W}_{M+1}^{(g_{M+1})}$ is un-bolded to distinguish it as the primary prediction.

In addition to utilizing past disturbance information, the proposed IL prediction algorithm also makes use of the error in past predictions. This is done by comparing the primary prediction $\hat{W}_i^{(g_i)}$ for each iteration with the actual disturbance $W_i^{(g_i)}$ once the iteration has occurred. Specifically, the error in the primary prediction for iteration i is defined as

$$E_i^{(g_i)} := \left(W_i^{(g_i)} - \hat{W}_i^{(g_i)} \right) \oslash \hat{W}_i^{(g_i)}, \tag{4.10}$$

where $\oslash$ denotes element-wise division. A set of the error in the primary prediction of the last D_α disturbance iteration vectors belonging to group g and occurring on or before iteration M can then be defined as $\mathcal{E}_{M,D_\alpha}^{(g)}$. The resulting error in past primary predictions is then incorporated in the final disturbance trajectory prediction algorithm, which is proposed as:

$$\hat{\boldsymbol{W}}_{M+1}^{(g_{M+1})} = \left[\begin{array}{cccc} \hat{w}_1, & \hat{w}_2, & \dots, & \hat{w}_{k_f} \end{array} \right] = \alpha_{M+1}^{(g_{M+1})} \odot \hat{W}_{M+1}^{(g_{M+1})}, \tag{4.11}$$

where

$$\alpha_{M+1}^{(g_{M+1})} := \vec{1} + A \left\{ \mathcal{E}_{M,D_\alpha}^{(g_i)} \right\}, \tag{4.12}$$

and $\odot$ denotes element-wise multiplication. As a whole, $\alpha_{M+1}^{(g_{M+1})} \in \mathbb{R}^{k_f}$ is a vector representing the average percentage error in the disturbance prediction at each time over the past D_α iterations of group g_{M+1}. It is used to account for trends, such as seasonal trends, in the disturbance data that lead to consistent errors in primary disturbance predictions. Since the goal of $\alpha_{M+1}^{(g_{M+1})}$ is to correct for consistent errors, all past errors are of equal importance and no weighting is used in (4.12). Random errors not exhibiting any particular trend have little impact on $\alpha_{M+1}^{(g_{M+1})}$ as they tend to cancel each other out in the averaging function [50].

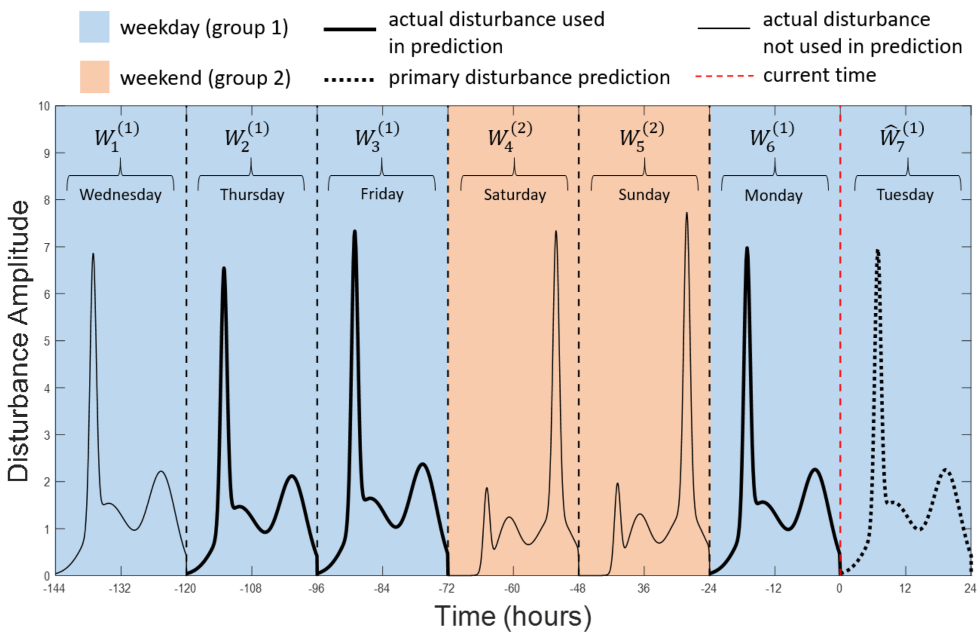

Figure 4.2: Demonstration of grouping and primary disturbance prediction

4.3.1 Primary Prediction

In order to better understand the primary prediction algorithm, let us circle back to the example given in Section 4.2 that features the disturbance iterations displayed in Fig. 4.2. As mentioned, the problem here is to predict the disturbance trajectory for the upcoming iteration based on the disturbances of the previous iterations. By choosing $D = 3$ and $\rho = \begin{bmatrix}1, & 1, & 1\end{bmatrix}$ in (4.9) the predicted disturbance trajectory, which is also displayed in Fig. 4.2, can be obtained. In accordance with (4.9), this primary prediction (dotted black curve) is taken as an average of the previous 3 disturbance iterations belonging to group $g = 1$, which encompasses the iterations falling on weekdays.

4.3.2 Final Prediction

Now, to help visualize the functionality of the proposed final prediction algorithm, a second disturbance prediction example is illustrated in Fig. 4.3. In this figure, an arbitrary disturbance profile (blue curve) is assumed to vary steadily with each 24 hour iteration. For simplicity all iterations here are considered to be in the same group, and values of $D = 1$ and $D_\alpha = 1$

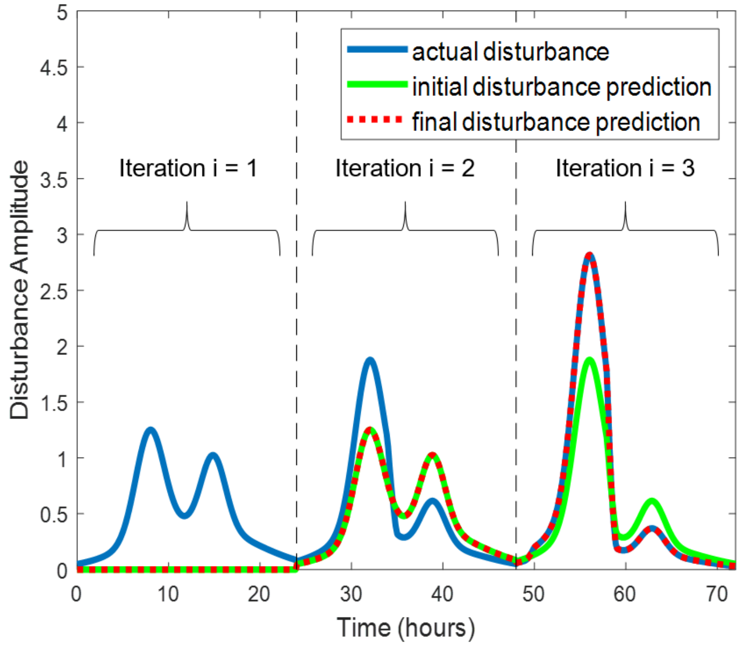

Figure 4.3: Demonstration of final IL prediction algorithm

are implemented in (4.9) and (4.12). During the first iteration, previous disturbance data is stored in memory and used to make disturbance predictions for iteration $i = 2$. At this point, the initial and final disturbance predictions are identical as there is not yet any information available on the prediction error of past iterations. After the second iteration, the error in the initial prediction can then be calculated and used to adjust the final prediction for iteration $i = 3$. As expected, this final prediction matches the actual disturbance trajectory for iteration $i = 3$ perfectly while the initial prediction once again lags behind the trend.

4.4 Memory Requirements

In order to run the proposed IL disturbance prediction algorithm, some memory is required to store past disturbance iterations as well as past primary disturbance predictions. As a whole the exact amount of memory required will depend on user choices for D and D_α as well as the number of groups G in the disturbance data, but in general the requirements should be quite reasonable. Assuming each data point can be stored as a floating point number, and noting that it takes approximately 4 bytes to store one floating point number in memory, it can be proven that the total storage required by the proposed IL disturbance prediction algorithm is either $4Gk_f(D + D_\alpha)$ bytes or $8Gk_fD_\alpha$ bytes depending on the choices of D and D_α.

Theorem 1. *The memory storage requirement for the proposed IL disturbance prediction algorithm is $4Gk_f(D + D_\alpha)$ bytes if $D < D_\alpha$ and $8Gk_fD_\alpha$ bytes if $D_\alpha \geq D$.*

Proof. Solely considering past disturbance iterations, it can be seen by looking at (4.9) that for each group $g_i \in \{1, \ldots, G\}$ the past D must be stored, with each iteration containing k_f discrete data points. Looking now to (4.11), the previous D_α disturbance iterations for each group must be stored. Since both (4.9) and (4.11) require the storage of a number of previous disturbance iterations, the exact amount of iterations needed can be determined by multiplying Gk_f by the larger of D and D_α.

In addition, (4.11) requires the storage of the last D_α primary predictions for each group. Each of these primary predictions also have k_f discrete data points, leading to a total storage requirement for past primary predictions of Gk_fD_α.

Adding the storage requirements for previous disturbance iterations to those for previous primary predictions leads to a memory storage requirement of either $Gk_f(D + D_\alpha)$ data points if $D > D_\alpha$ or $2Gk_fD_\alpha$ data points if $D_\alpha \geq D$. Finally, factoring in 4 bytes of storage for each data point leads to a total memory storage requirement of $4Gk_f(D + D_\alpha)$ bytes if $D > D_\alpha$ and $8Gk_fD_\alpha$ if if $D_\alpha \geq D$. $\square$

4.5 Validity of the Proposed Disturbance Prediction Method

In this subsection, it will be shown that the proposed disturbance prediction algorithm (4.11) eventually generates a prediction $\hat{\boldsymbol{W}}_i^{(g_i)}$ which exactly matches the actual disturbance $W_i^{(g_i)}$, under the condition that the iterations within group g_i exhibit steadily varying disturbances. This property supports the validity of the proposed IL-based disturbance prediction method.

Let us say there exists a series $\mathcal{S}$ containing M disturbance iterations grouped into a single group g:

$$\mathcal{S} := \left[W_1^{(g)}, \quad W_2^{(g)}, \quad \ldots, \quad W_M^{(g)} \right]. \tag{4.13}$$

Let us further assume that after some disturbance iteration i the disturbance iterations in $\mathcal{S}$ begin to exhibit repetition along with a steady shift quantified by:

$$W_{i+k}^{(g)} = \beta^{ok} \odot W_i^{(g)}. \tag{4.14}$$

Here $k \in \mathbb{Z}_+$ represents the number of iterations that have passed. Further, $\beta \in \mathbb{R}^{k_f}$ is the steady shift operator, and ^{o} denotes an element-wise power. In this case it can be proven that the convergence of the proposed disturbance prediction method to the actual disturbance can be guaranteed in a finite number of iterations. Note that this set up with only a single group g is without loss of generality in the sense that the same result can be proven as long as the iterations in group g exhibit the steady shift property, regardless of how many groups G there are.

Theorem 2. *The prediction algorithm given in (4.11) is such that* $\forall \mathcal{S} \in \mathbb{R}^{M \times k_f}, \forall D,\, D_\alpha \in \mathbb{Z}_+, \forall \rho \in \mathbb{R}_+^D, \forall c \in \mathbb{Z}_+ \mid c \geq (D+D_\alpha)$*, the final prediction* $\hat{\boldsymbol{W}}_{i+c}^{(g)} = W_{i+c}^{(g)}$.

Proof. The proof can be completed by expanding and simplifying the final disturbance prediction algorithm based on the stated conditions.

To begin, $\hat{W}_{i+c}^{(g)}$ is expanded:

$$\begin{aligned}
\hat{W}_{i+c}^{(g)} &= A_\rho \left\{ \mathcal{W}_{i+c-1,D}^{(g)} \right\} \\
&= A_\rho \left\{ (\beta^{o(c-1)} \odot W_i^{(g)}, \ldots, \beta^{o(c-D)} \odot W_i^{(g)} \right\} \\
&= A_\rho \left\{ \beta^{o(D-1)}, \ldots, 1 \right\} \odot \beta^{o(c-D)} \odot W_i^{(g)}
\end{aligned} \tag{4.15}$$

Next, $\alpha_{i+c}^{(g)}$ is expanded:

$$
\begin{aligned}
&\alpha_{i+c}^{(g)} = \vec{1} + A\left\{\mathcal{E}_{i+c-1,D_\alpha}^{(g)}\right\} \\
&\alpha_{i+c}^{(g)} = \vec{1} + A\left\{E_{i+c-1}^{(g)}, \ldots, E_{i+c-D_\alpha}^{(g)}\right\} \\
&\alpha_{i+c}^{(g)} = \vec{1} + A\left\{\left(W_{i+c-1}^{(g)} - \hat{W}_{i+c-1}^{(g)}\right) \oslash \hat{W}_{i+c-1}^{(g)}, \ldots,\right. \\
&\qquad \left.\left(W_{i+c-D_\alpha}^{(g)} - \hat{W}_{i+c-D_\alpha}^{(g)}\right) \oslash \hat{W}_{i+c-D_\alpha}^{(g)}\right\} \\
&\alpha_{i+c}^{(g)} = \vec{1} + A\left\{W_{i+c-1}^{(g)} \oslash \hat{W}_{i+c-1}^{(g)} - \vec{1}, \ldots, W_{i+c-D_\alpha}^{(g)} \oslash \hat{W}_{i+c-D_\alpha}^{(g)} - \vec{1}\right\} \\
&\alpha_{i+c}^{(g)} = A\left\{W_{i+c-1}^{(g)} \oslash \hat{W}_{i+c-1}^{(g)}, \ldots, W_{i+c-D}^{(g)} \oslash \hat{W}_{i+c-D_\alpha}^{(g)}\right\} \\
&\alpha_{i+c}^{(g)} = A\left\{\beta^{o(c-1)} \odot W_i^{(g)} \oslash \left(A_\rho\left\{\beta^{o(D-1)}, \ldots, 1\right\} \odot \beta^{o(c-D-1)} \odot W_i^{(g)}\right),\right. \\
&\qquad \left.\ldots, \beta^{o(c-D_\alpha)} \odot W_i^{(g)} \oslash \left(A_\rho\left\{\beta^{o(D-1)}, \ldots, 1\right\} \odot \beta^{o(c-D-D_\alpha)} \odot W_i^{(g)}\right)\right\} \\
&\alpha_{i+c}^{(g)} = A\left\{\beta^{o(D)} \oslash A_\rho\left\{\beta^{o(D-1)}, \ldots, 1\right\}, \ldots, \beta^{o(D)} \oslash A_\rho\left\{\beta^{o(D-1)}, \ldots, 1\right\}\right\} \\
&\alpha_{i+c}^{(g)} = \beta^{o(D)} \oslash A_\rho\left\{\beta^{o(D-1)}, \ldots, 1\right\}
\end{aligned}
\tag{4.16}
$$

The transition from line 5 to 6 in (4.16) follows from the fact that $i + c - D - D_\alpha \geq i$. Since the oldest disturbance iteration considered in (4.16) is $W_{i+c-D_\alpha-D}^{(g)}$ it is therefore clear that all iterations considered abide by (4.14). Finally, in order to arrive at the final disturbance prediction in (4.11) , (4.16) must be multiplied element wise by (4.15):

$$
\begin{aligned}
\hat{\boldsymbol{W}}_{i+c}^{(g)} &= \alpha_{i+c}^{(g)} \odot \hat{W}_{i+c}^{(g)} \\
&= \left(\beta^{o(D)} \oslash A_\rho\left\{\beta^{o(D-1)}, \ldots, 1\right\}\right) \odot \\
&\quad \left(A_\rho\left\{\beta^{o(D-1)}, \ldots, 1\right\} \odot \beta^{o(c-D)} \odot W_i^{(g)}\right) \\
&= \beta^{o(c)} \odot W_i^{(g)} \\
\hat{\boldsymbol{W}}_{i+c}^{(g)} &= W_{i+c}^{(g)}
\end{aligned}
$$

□

This theorem demonstrates why the proposed prediction algorithm is effective in the case of quasi-repetitive disturbances. Note that, in the case where the assumptions used in Theorem 2 hold, the best choice for D and

D_α will always be 1, as this choice guarantees the fastest convergence. In reality though, disturbance profiles are unlikely to exhibit perfect repetition or perfectly steady shifts. In such imperfect scenarios, D and D_α can be adjusted to average over more iterations, leading to predictions that are more robust to disturbance fluctuations.

Chapter 5

Intelligent Grouping

In Chapter 4, by assuming that the groups $\{1, \ldots, G\}$ for disturbance iterations were known, an IL-based method for future disturbance trajectory prediction was presented. In this section, a method for intelligently grouping past disturbance iterations will be proposed, along with a method for assigning groups to unknown future iterations. A high level overview of the intelligent grouping approach is first provided in Section 5.1. The specifics of the intelligent clustering are then detailed in Section 5.2 while various options for intelligent classification are finally explored in Section 5.3. Similarly to the previous chapter, this chapter describes the proposed intelligent grouping approach for disturbance iterations in a general manner. This approach is then applied specifically to grouping HWD iterations in the ISTS simulation detailed in Chapter 6

5.1 Overview

At a high level, the proposed intelligent grouping method begins by clustering a set of disturbance iterations, based on their disturbance trajectories themselves, into several groups. This is completed using the unsupervised learning method *k-means* as shown by the first arrow in Fig. 5.1. Each iteration is then paired with corresponding measurable features, such as day of the week and average temperature of the day, so that every iteration has both a set of features and a group label. This process corresponds to the second arrow in Fig. 5.1. The data set is further split into testing and training sets and multiple supervised learning classifiers are trained on the training set to map from features to group label; see the third arrow in Fig. 5.1. The best supervised learning approach for the given data set is then determined based on the performance of all the trained classifiers on the test set. Finally, future iterations are classified with this 'best' classifier, allowing the IL prediction algorithm in (4.11) to be applied. This step is depicted by the final arrow in Fig. 5.1.

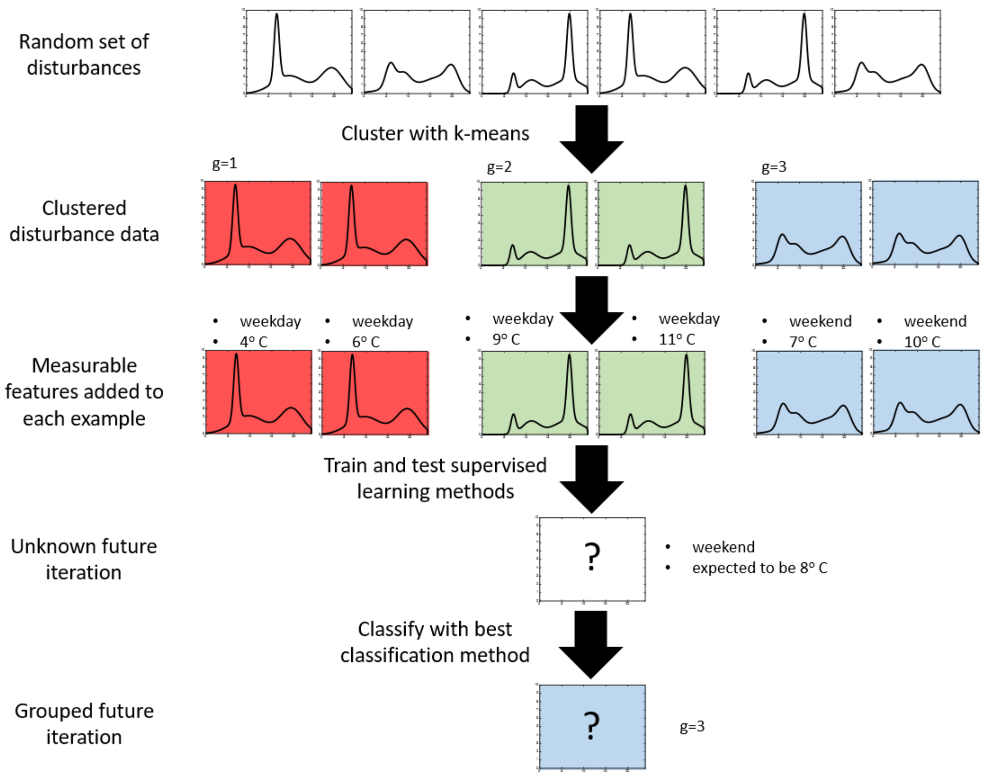

Figure 5.1: Visual representation of proposed approach to intelligent grouping

5.2 Clustering

Examining the initial IL prediction algorithm in (4.9), it is evident why intelligent grouping is necessary for improved disturbance prediction. The prediction is based on a weighted average of the past D iterations of group g. As a result, the smaller the Euclidean distance between the past D iterations and the upcoming iteration of group g, the more accurate the prediction. By grouping the iterations intelligently, this distance can be lowered within every group and a reduced prediction error can be achieved. The grouping process is referred to as clustering, which is a type of unsupervised machine learning.

The clustering algorithm implemented in this research is *k-means* clustering. This is the most widely used clustering algorithm and was selected due to its relative simplicity, allowing it to be effectively applied to many fields [51–55]. The algorithm attempts to separate a set of examples into k clusters, with k being a hyper-parameter. In this research, the features for clustering are the disturbance values at each time step of a disturbance iteration.

The main issue with regard to the *k-means* algorithm is selecting the ideal number of means k. Note that in this case k is synonymous with the number of groups G. The most commonly applied approaches for optimizing k are termed the *elbow method* [56] and the *gap statistic method* [57], with the former being a simple visual tool and the latter being a more sophisticated approach. In this research, the gap statistic method is used as it allows the optimal k value to be determined even in the case when no clear value presents itself visually through the elbow method, thus rendering it more generally applicable [57].

5.3 Classification

After clustering the past M disturbance iterations $W_1, \ldots, W_M$ into G groups, the remaining issue is determining which group g_{M+1} the next iteration $M+1$ belongs to. This is necessary in order to make a disturbance prediction $\hat{\boldsymbol{W}}_{M+1}^{(g_{M+1})}$ for iteration $M+1$, based on the proposed IL prediction algorithm in (4.11). The process of determining the group of a future iteration is referred to as *classification*, which is a type of supervised machine learning. In the case of naive clustering where groups are determined based on a single feature, classification is simple and can be completed in the same naive manner. In the case of intelligent clustering however, the nature of the groups is much more abstract and an intelligent classification method is required.

With the clustering complete and all disturbance iterations labeled, a supervised learning classifier must be trained on the data. In the clustering section, the features for each iteration simply consisted of disturbance data. However, since future disturbance data is unknown, new features are required for each disturbance iteration. The exact features used for a given ISTS application will of course be case-dependent, but some possible features include things such as day of the week, work day or holiday, and month of the year.

Once features are in place, the ideal type of classification method must be determined. The no-free-lunch theorem of supervised learning states there is no ultimate supervised learning approach, with some algorithms working better for certain problems and other algorithms proving superior on other problems [58]. With this theorem in mind, a number of methods should be examined for any given application. While hundreds of supervised learning algorithms exist, a good starting point is to explore some of the top ranked classifiers presented by Delgado et al. [59].

In order to evaluate the effectiveness of the different methods, training and testing sets must be allocated. In this research two thirds of the available data will be randomly selected and held in a training set while the remaining third is put aside for testing. Further, the various hyper-parameters for the different supervised learning models will be tuned with an effective method called *k-fold cross-validation* [60]. After hyper-parameter tuning, each classifier is then trained on the entire training set and tested on the test set.

The model with the best performance in the test set is then selected for actual use in the disturbance iteration classification, assuming this best performance is up to an adequate standard. The level of performance that constitutes 'adequate' will depend on the specific application and can be confirmed on a case-by-case basis by exploring the prediction ability of the resulting IL prediction algorithm on the test set data. In the case of inadequate performance, adjustments can be made such as updating the features. Once a specific method is selected, the model is trained one last time on the entire data set. It is then incorporated into the IL process and used online to predict the group of upcoming disturbance iterations. Note that after an iteration is complete, it is then grouped based on its actual disturbance data, as opposed to its predicted group, for use in future disturbance prediction.

Chapter 6

Simulation

A computer simulation is included to demonstrate the effectiveness of the proposed method for disturbance prediction within EMPC on an ISTS control problem. The benefits of the proposed method are evaluated relative to other common disturbance prediction approaches both in terms of the disturbance prediction itself and the corresponding controller performance.

6.1 Simulation Settings

6.1.1 Component Specifics

The specific ISTS used in the simulation features a Seido 1-16 STC, a cylindrical TST with a volume of 200 L, and a three-stage auxiliary HP with 3 kW of power set up in a parallel fashion as seen in Fig. 2.1. The system has three loops, each containing a pump to circulate the fluid inside. The control objective for the ISTS in this simulation is to maintain the top layer temperature in the TST between 60^0C and 75^0C by regulating the compressor speed ratio of the HP (O1) while minimizing energy costs (O2). These temperature limits are based on the building code for domestic hot water in Canada. The operating cost of the HP at a given time is a function of the cost of electricity at that time. Canadian electrical time-of-use price periods in Table 6.1 are adopted for this simulation.

Table 6.1: Time-of-use electrical price periods

Time of day (hours)	0-7	7-11	11-17	17-19	19-24
Cost (¢/kWh)	6.5	9.4	13.4	9.4	6.5

6.1.2 Model Parameters

For this simulation a 7-state version of the general discrete-time nonlinear state space model shown in (2.2) is implemented:

$$T_{k+1} = f(T_k, u_k, w_k), T \in \mathbb{R}^7. \tag{6.1}$$

Here the state vector consists of fluid temperatures at seven different locations in the glsists, denoted by the temperature sensors in Fig. 2.1. The full equation for the specific state space model used in the simulation can be seen in the Appendix. Note that the model in the Appendix is a continuous-time model that was discretized before being used in the simulation.

6.1.3 Disturbance Description

The disturbance data used in this simulation is real domestic hot water consumption flow rate data taken at 1 minute intervals over an entire year. The data is taken from [33] for a specific house in Halifax, Canada over the period of time from July 31$^{\text{st}}$, 2014 to July 30$^{\text{th}}$, 2015. The average daily consumption profile seen in the data for this house over the course of the year is displayed in Fig. 6.1.

6.1.4 Disturbance Prediction

In this subsection the disturbance prediction algorithms specific to this case study are detailed. In addition to the method proposed in this research, a few other common disturbance prediction methods are explored for comparison purposes. Note that the simulation detailed in Section 6.1.5 simulates controller performance for 2 random days from each month and as such the data for these 24 days are withheld from the prediction algorithm development process. That leaves 341 days of data to work with for training and tuning various aspect of the prediction methods outlined below.

Iterative Learning With Intelligent Grouping

This is the approach presented in this research based on the prediction algorithm proposed in Chapter 4 and the grouping method proposed in Chapter 5. The disturbance data was initially sorted into disturbance iterations, with one iteration for each day, and the *k-means* algorithm was applied. Based on the *gap statistic method* it was determined that the number of groups $G = 5$. The resulting 5 mean consumption profiles can be seen in Fig. 6.2.

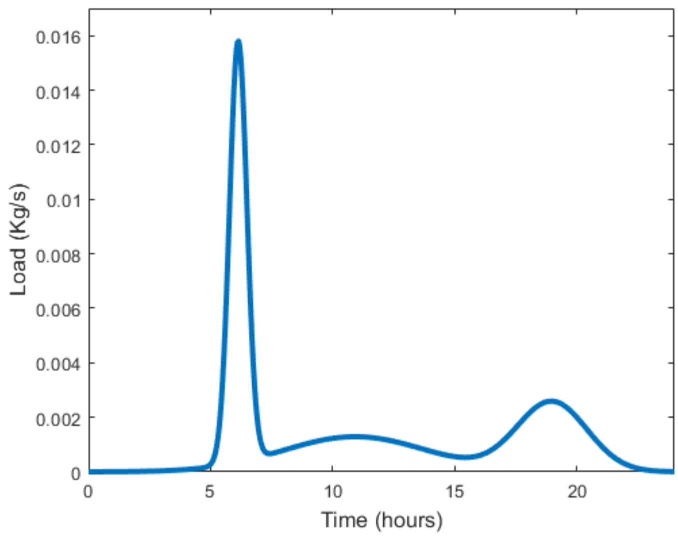

Figure 6.1: Average dialy hot water consumption profile for a house in Halifax, Canada

Upon completing the grouping, new features were assigned to each HWD iteration. The selected features were day of the week, month of year, whether or not the day is a holiday, the average visibility [km], the average temperature [^{o}C], the average humidex index, and the average wind-chill index. Historical weather data for Halifax, Canada was obtained from [61]. The data was then randomly split into training and testing sets with two thirds for training and one third for testing. The following 6 classification methods were then trained on the training set with 5-fold cross-validation for hyper-parameter tuning:

ANN Artificial Neural Network

RF Random Forests

AB Adaboost

GB Gaussian Boosting

SVM Support Vector Machines

KNN K-Nearest Neighbors

Note that all algorithms were implemented in Python using the scikit-learn library. The trained algorithms were then tested on the test set based on

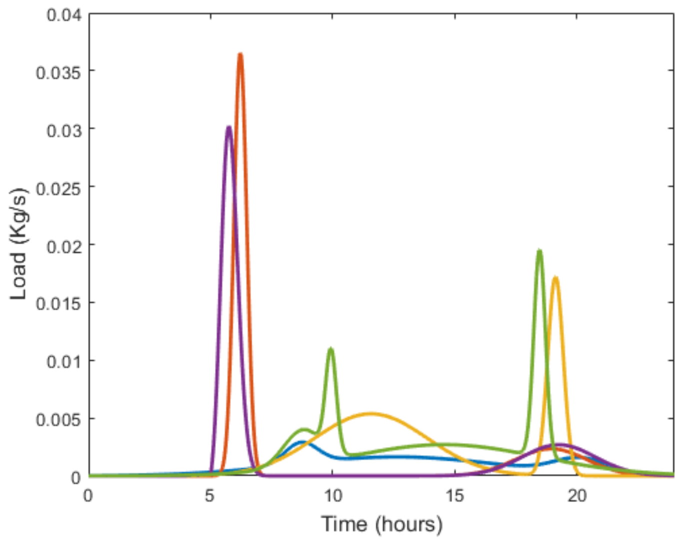

Figure 6.2: The 5 mean hot water consumption profiles

their ability to correctly classify disturbance iterations by group. Testing results are depicted in Table 6.2.

Table 6.2: Performance of various supervised classification methods

Classification Method	ANN	RF	AB	GB	SVM	KNN
Training Accuracy (%)	80	100	77	89	98	100
Test Accuracy (%)	73	86	68	77	57	56

From the results it is clear that RF is the optimal classification method in this case study, correctly classifying 86% of the unseen test examples. As a result, RF was implemented for group predication. The specific random forests model selected through cross-validation uses 1000 trees and considers 3 features for each split.

Methods For Comparison

Iterative Learning With Naive Grouping: The prediction algorithm used in this approach is again the algorithm proposed in Chapter 4. The difference here is that iterations are grouped naively based on a single measurable feature. The feature used in this case is the day of the week, generating seven groups $G = 7$. There is evidence that hot water consumption data is fairly repetitive for specific days of the week which is why this feature is chosen over others [28].

ARANN: The specific ARANN approach used in this case study is the most recently published general approach for applications across a wide number of problem types [25] and is presented by Wang et al. in [62]. The described multiplicative hybrid strategy was trained on the same training set used in Section 6.1.4. A 5-fold cross-validation approach was then taken for hyper-parameter tuning.

Average Profile: This approach simply uses the average consumption profile seen in Fig. 6.1 for prediction. This method is common in past research into EMPC with disturbance based on human consumption and provides a good baseline for both prediction and control performance [43, 44, 63, 64].

Perfect Prediction: The final prediction method is included to act as a performance ceiling and simply predicts the future disturbances perfectly. It is useful for determining how close the proposed method's performance is to optimal.

6.1.5 Controller Settings

In order to verify the effectiveness of the proposed disturbance prediction approach to EMPC with regards to this case study, a simulation was carried out in Matlab comparing the performance of five different economic model predictive controllers, each using a different prediction method outlined in Section 6.1.4. The specific EMPC scheme used is the one detailed in (3.1), (3.2), and (3.3) with $N = 12$ hours, $\mathcal{U} := [0, 1]$, $\underline{\eta} = 100$ and $\bar{\eta} = 0$. The prediction horizon is set at 12 hours to allow the controller sufficient time to react to upcoming hot water consumption rate changes and the 3 kW input capacity is scaled between 0 and 1. A time step of 15 minutes is also implemented in the EMPC scheme. For each controller the designed EMPC was implemented in MATLAB using SQP based on the *fmincon* function for solving the optimization problem at each iteration. Also note that the optimal control inputs were applied to the three-stage HP using the PWM approach detailed in Section 3.3.1. For simplicity, the five different controllers are denoted as follows:

(IIL) IL with intelligent grouping
(NIL) IL with naive grouping

(ARC) ARANN prediction

(A) Average profile prediction

(P) Perfect prediction

For (IIL) and (NIL) values of $D = 5$ and $\rho = \begin{bmatrix}1.25 & 1.25 & 1 & 1 & 1\end{bmatrix}$ are used in (4.9) while $D_\alpha = 3$ is used in (4.12).

Two days were randomly selected from every month of available data and the performance of each controller was evaluated on these days in the simulation. As mentioned, the rest of the available data was set aside for use in training the prediction methods. The selected days are displayed in Table 6.3, where the months start from August 2014 through to July 2015.

Table 6.3: Selected days for control performance simulation

Month	Aug	Sep	Oct	Nov	Dec	Jan
Days	4, 17	2,8	12,28	7,30	11,16	8,31
Month	Feb	Mar	Apr	May	Jun	Jul
Days	3,20	9,18	6,24	22,25	16,22	5,9

Finally, the solar radiation data used on each simulated day is based on a mathematical model of the solar radiation profile for Halifax, Canada on said day of the year [65].

6.2 Simulation Results

Prediction results for the various disturbance prediction methods outlined in Section 6.1.4 are detailed in Section 6.2.1 while the performance results of the corresponding controllers are displayed in Section 6.2.2.

6.2.1 Prediction

As a precursor to the control simulation results, the four non-perfect disturbance prediction methods outlined in Section 6.1.4 were compared based purely on their disturbance profile prediction ability. They were each tested on the 114 days featured in the test set from Section 6.1.4 with their performance evaluated based on the Euclidean distance between their predictions and the true disturbance profiles. This evaluation is a measure of prediction error and is described mathematically by

$$\text{Err} = \sum_{j \in \mathcal{T}_{est}} \|\hat{\boldsymbol{W}}_j - W_j\|^2, \tag{6.2}$$

where $\mathcal{T}_{est}$ is the test set containing 114 disturbance iterations. Note that for all methods it was assumed that data for previous days not included in the test set was available for prediction. Also note that the average daily hot water consumption for this household is 121.07 kg. The results of the test can be seen in Table 6.4.

Table 6.4: Error in prediction over 114 day test set

Prediction method	IL w/ intelligent grouping	IL w/ naive grouping	ARANN	Average profile
Total error (kg)	365.90	463.08	591.95	519.21
Avg daily error (kg)	3.21	4.06	5.19	4.55

The proposed prediction method clearly outperforms all other methods, decreasing prediction error by approximately 27% relative to the second best prediction method. It is also interesting to note that the ARANN prediction performs worse than even the average profile prediction method, indicating that despite its benefits in some fields, this modern style of time series prediction is not suitable for making long range predictions relative to the time step.

6.2.2 Control Performance

Complete results for the controller simulations are summarized in Table 6.5, where the important performance metrics to consider are cost, average constraint violation (ACV), and average daily maximum constraint violation (AMCV). Disturbance profile prediction and output temperature plots for December 16th, 2014 and March 18th, 2015 are then displayed in Fig. 6.3 and Fig. 6.4 respectively. The plots for December 16th, 2014 depict the results in the case when the disturbance profile is fairly typical and (IIL) performs comparatively to the other controllers. The March 18th, 2015 plots then show the case when the disturbance is "unusual" and (IIL) greatly outperforms the other controllers. In this ISTS application typical disturbance profiles feature a HWD peak in the morning, much like the average disturbance profile in Fig. 6.1, while unusual disturbance profiles have HWD peaks at other times of the day or no distinct peak at all.

Table 6.5: Performance results of examined controllers

Controller	P	IIL	NIL	ARC	A
Avg daily cost ($)	2.17	2.19	2.33	2.52	2.36
Deviation (%)	-	0.92	7.37	15.98	8.76
ACV (°C)	0.036	0.040	0.057	0.093	0.059
Deviation (%)	-	11.11	58.33	158.33	63.89
AMCV (°C)	0.64	0.71	1.04	1.55	1.14
Deviation (%)	-	10.94	62.50	142.19	78.13

Examining Table 6.5, it is clear that (IIL) performed nearly as well as (P), while outperforming the other control strategies in every category. Most notably, while outperforming all non-idealistic controllers with regards to constraint violations, (IIL) reduced the average daily cost relative to the next best controller by 6.01%.

By looking at Fig. 6.3 and Fig. 6.4, it is apparent that (IIL) was able to manage the ISTS output temperature quite effectively while limiting cost. Looking to Fig. 6.3a it can be seen that all methods aside from (ARC) predict similar consumption profiles, only varying in amplitude. As a result the output plot for these methods in Fig. 6.3b depicts comparable performance across the board, with (IIL) performing slightly more efficiently than other non-deal controllers by not heating the system unnecessarily thanks to the improved amplitude accuracy in its prediction.

Next, looking to Fig. 6.4a it can be seen that (IIL) is the only controller that predicts a load profile somewhat resembling the actual load. The importance of this prediction accuracy is revealed in Fig. 6.4b, where (NIL) and (A) do no sufficiently preheat the system between hours 10 and 18 ahead of the load peak at hour 18 since they don't expect it. Since (IIL) is able to predict the load trajectories with greater accuracy, it avoids this problem. Meanwhile, the prediction for (ARC) is so far off from hours 5 to 15 that heavy constraint violations are already incurred before the peak at 18 hours even arrives.

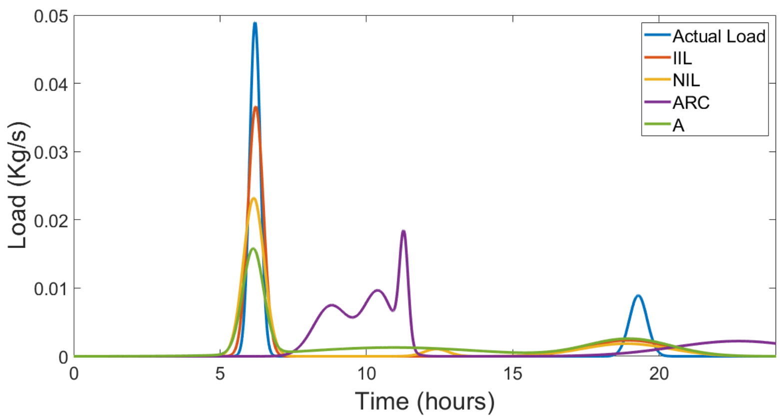

(a) Hot water consumption profile prediction

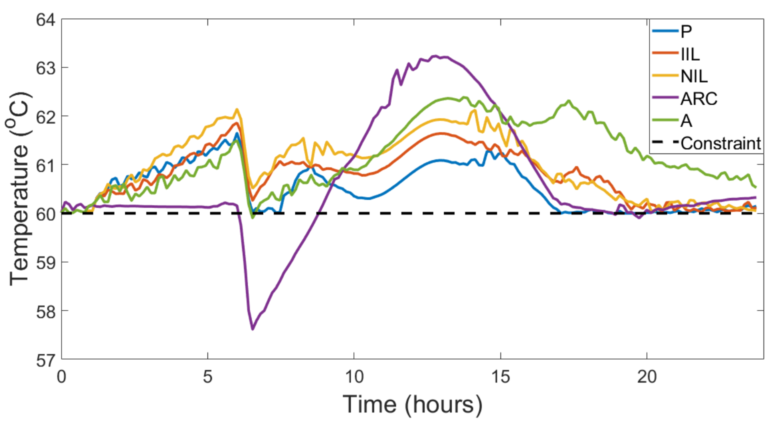

(b) Top layer temperature of the TST

Figure 6.3: Performance of various controllers on December 16th, 2014

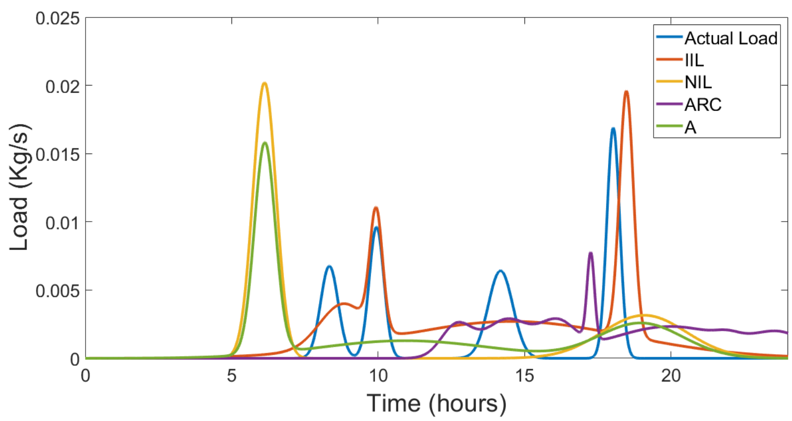

(a) Hot water consumption profile prediction

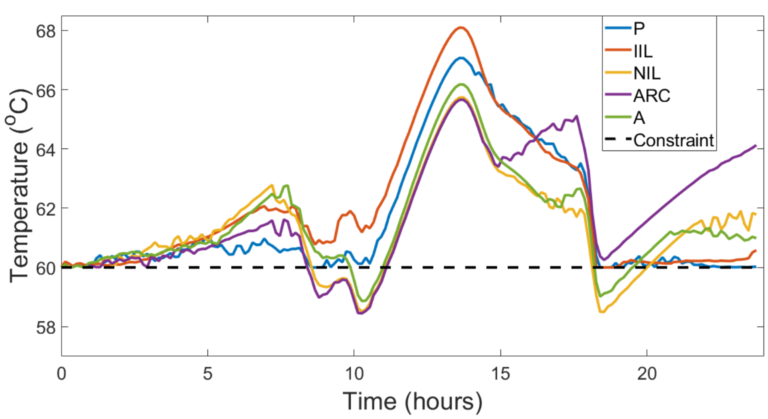

(b) Top layer temperature of the TST

Figure 6.4: Performance of various controllers on March 18th, 2015

Chapter 7

Conclusion and Future Works

7.1 Summary

This thesis presented a novel IL approach to disturbance prediction in EMPC for an ISTS. The proposed approach also incorporated intelligent iteration grouping for improved functionality through the use of both supervised and unsupervised machine learning techniques. The goal of this IL-based approach was to improve the accuracy of prediction in the EMPC relative to existing methods so as to allow it achieve a higher level of control performance in the ISTS. This higher level control performance is quantified by maintaining the system output within a desired temperature range while minimizing electrical costs relative to EMPC implementations using other disturbance prediction approaches.

In Chapter 2 of the thesis a description of the ISTS to be considered in this research was given. This ISTS consists of an STC which collects energy from the sun, a TST which stores this energy for later use, and an auxiliary HP which provides additional heat energy as needed. The control input for the system actuates the HP by setting the compressor speed ratio. Mathematical descriptions of all the system components were also detailed in Chapter 2, leading to the development of discrete-time nonlinear state space model for the ISTS. The control objectives of the system were then explained in Chapter 3 and the EMPC strategy was designed. A PWM approach was also proposed in this chapter, allowing the EMPC strategy to be implemented in cases where a variable speed HP is not available.

The IL algorithm for disturbance prediction in EMPC was then proposed in Chapter 4, and validated with Theorem 2. This algorithm consists of a primary prediction algorithm that iteratively analyzes past disturbance iterations as well as a final prediction algorithm that analyses the error in past disturbance predictions. Next, the grouping aspect of the IL algorithm was further explored in Chapter 5, and a procedural approach to iteration clustering and classification using machine learning was described.

Finally, an ISTS simulation using real domestic hot water consumption data was presented in Chapter 6. This simulation demonstrated the efficiency of the proposed IL-based approach to disturbance prediction in EMPC relative to other disturbance prediction approaches. In the simulation the IL method was able to decrease HWD prediction error by 38% relative to the next best prediction strategy. This improved prediction accuracy led to heightened controller performance, as the EMPC implementation using the proposed IL method for disturbance prediction was able to avoid temperature constraint violations more effectively than all other EMPC implementations, while also decreasing the average daily system costs by over 6%.

7.2 Contribution

The main contribution of this research was to propose a novel IL-based disturbance prediction algorithm that works to improve EMPC performance to a level that cannot be achieved with existing disturbance prediction methods. This algorithm iteratively analyzes grouped disturbance iterations, recognizes patterns within each group, and uses these patterns to make disturbance predictions for future iterations. In order to improve the functionality of the algorithm, a machine learning based procedure to group the disturbance iterations intelligently was also proposed as a an additional contribution. This intelligent grouping approach utilizes both supervised and unsupervised machine learning techniques to group past disturbance iterations based on their disturbance trajectories and predict the groups of future disturbance iterations with unknown trajectories.

7.3 Future Works

There are a number of potential directions that could be taken for future work on this topic. From a theoretical perspective, it would be interesting to try and guarantee the stability of the ISTS when controlled with an EMPC scheme using the proposed disturbance prediction method. It would also be interesting to explore the impact of varying solar radiation. In this work it was assumed that that the solar radiation profile on a given day was known by the EMPC but in reality that is not the case. It would be useful to see what kind of impact error in the prediction of the solar radiation profile would have on the performance of the controller, and to come up with a strategy for improving the accuracy of that prediction.

From an experimental point of view, it would be nice to be able to confirm the results of this thesis in practice with real equipment. Work in this regard is already underway at the University of British Columbia, where there is a prototype solar thermal setup on the roof of the Centre for Interactive Research on Sustainability that can be seen in Fig. 7.1 below.

Figure 7.1: Experimental solar thermal setup at the University of British Columbia

Bibliography

[1] J. Mohtasham, Review article-renewable energies, Energy Procedia 74 (2015) 1289–1297.

[2] G. Crabtree, N. Lewis, Solar energy conversion, Physics Today 60 (03 2007).

[3] C. Aguilar, D. White, D. Ryan, Domestic water heating and water heater energy consumption in canada (2005).

[4] J. Archibald, Building integrated solar thermal roofing systems-history, current status and future promise, The Solar Conference, American Solar Energy Society (1999) 95–100.

[5] B. Greening, A. Azapagic, Domestic solar thermal water heating: A sustainable option for the uk?, Renewable Energy 63 (2014) 23–36.

[6] Y. Tian, C. Zhao, A review of solar collectors and thermal energy storage in solar thermal, Applied Energy 104 (2013) 538–553.

[7] M. Karagiorgas, A. Botzios, T. Tsoutsos, Industrial solar thermal applications in Greece: Economic evaluation, quality requirements and case studies, Renewable and Sustainable Energy Reviews 5 (2) (2001) 157–173.

[8] R. Halvgaard, P. Bacher, B. Perers, E. Andersen, S. Furbo, J. Jørgensen, N. Poulsen, H. Madsen, Model predictive control for a smart solar tank based on weather and consumption forecasts, Energy Procedia 30 (2012) 270 – 278.

[9] R. Godina, E. Rodrigues, E. Pouresmaeil, J. Matias, J. Catalão, Model predictive control home energy management and optimization strategy with demand response, Applied Sciences 8 (2018) 408.

[10] H. Weeratunge, G. Narsilio, J. de Hoog, S. Dunstall, S. Halgamuge, Model predictive control for a solar assisted ground source heat pump system, Energy 152 (03 2018).

[11] E. F. Camacho, C. Bordons, Model predictive control, Springer, 2007.

[12] M. Ellis, J. Liu, P. D. Christofides, Economic Model Predictive Control: Theory, Formulations and Chemical Process Applications, Springer International Publishing, 2018.

[13] T. Broomhead, C. Manzie, P. Hield, R. Shekhar, M. Brear, Economic model predictive control and applications for diesel generators, IEEE Transactions on Control Systems Technology 25 (2) (2017) 388–400.

[14] J. Zeng, J. Liu, Economic model predictive control of wastewater treatment processes, Industrial & Engineering Chemistry Research 54 (21) (2015) 5710–5721.

[15] J. Ma, J. Qin, T. Salsbury, P. Xu, Demand reduction in building energy systems based on economic model predictive control, Chemical Engineering Science 67 (1) (2012) 92–100.

[16] R. Halvgaard, N. K. Poulsen, H. Madsen, J. B. Jorgensen, Economic model predictive control for building climate control in a smart grid, 2012 IEEE PES Innovative Smart Grid Technologies (ISGT) (2012).

[17] S. Edwards, I. Beausoleil-Morrison, A. Laperrière, Representative hot water draw profiles at high temporal resolution for simulating the performance of solar thermal systems, Solar Energy 111 (2015) 43–52.

[18] M. Armstrong, M. C. Swinton, H. Ribberink, I. Beausoleil-Morrison, J. Millette, Synthetically derived profiles for representing occupant-driven electric loads in canadian housing, Journal of Building Performance Simulation 2 (03 2009).

[19] Y. Ma, Predictive control for energy efficient buildings with thermal storage: Modeling, stimulation, and experiments, IEEE Control Systems 32 (1) (2012) 44–64.

[20] A. Pawlowski, J. L. Guzman, F. Rodriguez, M. Berenguel, J. Sanchez, Application of time-series methods to disturbance estimation in predictive control problems, 2010 IEEE International Symposium on Industrial Electronics (2010).

[21] G. E. P. Box, G. M. Jenkins, G. C. Reinsel, G. M. Ljung, Time series analysis: forecasting and control, John Wiley & Sons, Inc., 2016.

[22] C. Bordons, J. Cueli, Predictive controller with estimation of measurable disturbances. application to an olive oil mill, Journal of Process Control 14 (3) (2004) 305–315.

[23] P. Doganis, E. Aggelogiannaki, H. Sarimveis, A combined model predictive control and time series forecasting framework for production-inventory systems, International Journal of Production Research 46 (24) (2008) 6841–6853.

[24] C.-C. Young, W.-C. Liu, W.-L. Hsieh, Predicting the water level fluctuation in an alpine lake using physically based, artificial neural network, and time series forecasting models, Mathematical Problems in Engineering 2015 (2015) 1–11.

[25] A. Tealab, Time series forecasting using artificial neural networks methodologies: A systematic review, Future Computing and Informatics Journal 3 (2) (2018) 334–340.

[26] B. Lupei, Advanced Model Predictive Control, Scitus Academics, 2016.

[27] P. Chronis, G. Giannopoulos, S. Athanasiou, Open issues and challenges on time series forecasting for water consumption, in: EDBT/ICDT Workshops, 2016.

[28] Department of Energy & Climate Change, Government of the United Kingdom, Measurement of domestic hot water consumption in dwellings, 2011.
URL `https://www.gov.uk/government/publications/measurement-of-domestic-hot-water-consumption-in-dwellings`

[29] D. H. Spennemann, Learning and teaching 24/7: daily internet usage patterns at nine australian universities, Campus-Wide Information Systems 24 (1) (2007) 27–44.

[30] J. Mikulik, Energy demand patterns in an office building: A case study in kraków (southern poland), Sustainability 10 (8) (2018) 2901.

[31] M. Chung, H.-C. Park, Building energy demand patterns for department stores in korea, Applied Energy 90 (1) (2012) 241–249.

[32] E. S. Trust, Measurement of domestic hot water consumption in dwellings, UK Department of Energy and Climate Change. (2008).

[33] D. George, N. S. Pearre, L. G. Swan, High resolution measured domestic hot water consumption of canadian homes, Energy and Buildings 109 (2015) 304–315.

[34] D. A. Bristow, M. Tharayil, A. G. Alleyne, A survey of iterative learning control, IEEE Control Systems Magazine 26 (3) (2006) 96–114.

[35] U. Rosolia, F. Borrelli, Learning model predictive control for iterative tasks. a data-driven control framework, IEEE Transactions on Automatic Control 63 (7) (2018) 1883–1896.

[36] K. S. Lee, I.-S. Chin, H. J. Lee, J. H. Lee, Model predictive control technique combined with iterative learning for batch processes, AIChE Journal 45 (10) (1999) 2175–2187.

[37] P.-C. Lu, J. Chen, L. Xie, Iterative learning control (ilc)-based economic optimization for batch processes using helpful disturbance information, Industrial & Engineering Chemistry Research 57 (10) (2018) 3717–3731.

[38] A. Nia, V. Grebenyuk, R. Nagamune, Modeling and control for an integrated thermal hydronic system, 2015 IEEE 28th Canadian Conference on Electrical and Computer Engineering (CCECE) (2015).

[39] M. Rostam, R. Nagamune, V. Grebenyuk, Switching gain-scheduled linear-quadratic-regulator control for integrated solar thermal hydronic systems, 2018 Annual American Control Conference (ACC) (2018) 2581–2586.

[40] A. Bemporad, M. Morari, Robust model predictive control: A survey, in: Robustness in identification and control, Springer London, London, 1999, pp. 207–226.

[41] C. Rao, S. Wright, J. Rawlings, Application of interior-point methods to model predictive control, Journal of Optimization Theory and Applications 99 (1998) 723–757.

[42] Q. Zhu, S. Onori, R. Prucka, Nonlinear economic model predictive control for si engines based on sequential quadratic programming, 2016 Annual American Control Conference (ACC) (2016) 1802–1807.

[43] H. Weeratunge, G. Narsilio, J. D. Hoog, S. Dunstall, S. Halgamuge, Model predictive control for a solar assisted ground source heat pump system, Energy 152 (2018) 974–984.

[44] R. Godina, E. Rodrigues, E. Pouresmaeil, J. Matias, J. Catalão, Model predictive control home energy management and optimization strategy with demand response, Applied Sciences 8 (3) (2018) 408.

[45] M. Pereira, D. M. D. L. Peña, D. Limon, Robust economic model predictive control of a community micro-grid, Renewable Energy 100 (2017) 3–17.

[46] S. Lucia, J. A. Andersson, H. Brandt, A. Bouaswaig, M. Diehl, S. Engell, Efficient robust economic nonlinear model predictive control of an industrial batch reactor, IFAC Proceedings Volumes 47 (3) (2014) 11093–11098.

[47] J. Dostál, L. Ferkl, Model predictive control of climatic chamber with on-off actuators, IFAC Proceedings Volumes (IFAC-PapersOnline) 19 (2014) 4423–4428.

[48] W. Burke, D. Auslander, Low-frequency pulse width modulation design for hvac compressors, Proceedings of the ASME Design Engineering Technical Conference 3 (01 2009).

[49] M. Avci, M. Erkoc, A. Rahmani, S. Asfour, Model predictive hvac load control in buildings using real-time electricity pricing, Energy and Buildings 60 (2013) 199–209.

[50] T. Lucey, Quantitative techniques, Thomson, 2004.

[51] Z. Kakushadze, W. Yu, K-means and cluster models for cancer signatures, SSRN Electronic Journal (2017).

[52] S. Ray, R. H. Turi, Determination of number of clusters in k-means clustering and application in colour segmentation, in: The 4th International Conference on Advances in Pattern Recognition and Digital Techniques, 1999, pp. 137–143.

[53] M. Jianliang, S. Haikun, B. Ling, The application on intrusion detection based on k-means cluster algorithm, in: 2009 International Forum on Information Technology and Applications, Vol. 1, 2009, pp. 150–152.

[54] Y. Liu, W. Li, Y. Li, Network traffic classification using k-means clustering, in: Second International Multi-Symposiums on Computer and Computational Sciences (IMSCCS 2007), 2007, pp. 360–365.

[55] C. Slamet, A. Rahman, M. Ramdhani, W. Darmalaksana, Clustering the verses of the holy qur'an using k-means algorithm, Asian Journal of Information Technology 15 (2016) 5159–5162.

[56] A. K. Jain, M. N. Murty, P. J. Flynn, Data clustering: a review, ACM Comput. Surv. 31 (1999) 264–323.

[57] R. Tibshirani, G. Walther, T. Hastie, Estimating the number of clusters in a data set via the gap statistic, Journal of the Royal Statistical Society: Series B (Statistical Methodology) 63 (2) (2001) 411–423.

[58] D. H. Wolpert, The Supervised Learning No-Free-Lunch Theorems, Springer London, London, 2002, pp. 25–42.

[59] M. Fernández-Delgado, E. Cernadas, S. Barro, D. Amorim, Do we need hundreds of classifiers to solve real world classification problems?, The Journal of Machine Learning Research 15 (1) (2014) 3133–3181.

[60] P. Refaeilzadeh, L. Tang, H. Liu, Cross-Validation, Springer US, Boston, MA, 2009, pp. 532–538.

[61] Climate change canada, government of canada / gouvernement du canada (Dec 2019).
URL `https://climate.weather.gc.ca/historical_data/search_historic_data_e.html`

[62] L. Wang, H. Zou, J. Su, L. Li, S. Chaudhry, An arima-ann hybrid model for time series forecasting, Systems Research and Behavioral Science 30 (3) (2013) 244–259.

[63] M. Rostam, R. Nagamune, V. Grebenyuk, Analysis of economic model predictive control parameters selection in an integrated solar thermal system, 2019 IEEE Conference on Control Technology and Applications (CCTA) (2019).

[64] M. A. A. Awadelrahman, Y. Zong, H. Li, C. Agert, Economic model predictive control for hot water based heating systems in smart buildings, Energy and Power Engineering 09 (04) (2017) 112–119.

[65] T. Khatib, W. Elmenreich, Modeling of photovoltaic systems using MATLAB®: simplified green codes, Wiley, 2016.

Appendix A

Supporting Materials

A.1 Closed Form State Space Model

In this section of the Appendix, the specific non-linear state space model for the case when the system model uses 7 states is provided. When containing 7 states, the state vector $\mathbf{T} \in \mathbb{R}^7$ takes the following form:

$$\mathbf{T} = \begin{bmatrix} \mathbf{T}^{(1)} \\ \mathbf{T}^{(2)} \\ \mathbf{T}^{(3)} \\ \mathbf{T}^{(4)} \\ \mathbf{T}^{(5)} \\ \mathbf{T}^{(6)} \\ \mathbf{T}^{(7)} \end{bmatrix}.$$

Here $\mathbf{T}^{(1)}$ is at the exit of the STC, $\mathbf{T}^{(2)}$ is at the entrance to the STC, $\mathbf{T}^{(3)}$ is at the exit of the HX in the TST loop, $\mathbf{T}^{(4)} = y$ is the output of the system which is at the top of the TST, $\mathbf{T}^{(5)}$ is in the middle of the TST, $\mathbf{T}^{(6)}$ is at the bottom of the TST, and $\mathbf{T}^{(7)}$ is at the exit of the HP. With that, the state space model itself becomes:

$$\begin{aligned}
\frac{d\mathbf{T}^{(1)}}{dt} &= \frac{\dot{Q}_{STC} + \dot{m}_{STC} C_{p,1}(\mathbf{T}^{(2)} - \mathbf{T}^{(1)})}{M_1 C_{p,1}} \\
\frac{d\mathbf{T}^{(2)}}{dt} &= \frac{\dot{m}_{STC} C_{p,2}(\mathbf{T}^{(1)} - \mathbf{T}^{(2)}) - U_{coil} A_{coil}(\mathbf{T}^{(2)} - \mathbf{T}^{(3)})}{M_2 C_{p,2}} \\
\frac{d\mathbf{T}^{(3)}}{dt} &= \frac{\dot{m}_{TST} C_{p,3}(\mathbf{T}^{(6)} - \mathbf{T}^{(3)}) + U_{coil} A_{coil}(\mathbf{T}^{(2)} - \mathbf{T}^{(3)})}{M_3 C_{p,3}} \\
&\quad - \frac{U_{shell} A_{shell}(\mathbf{T}^{(3)} - T_{amb})}{M_3 C_{p,3}}
\end{aligned}$$

(continued on next page)

(continued from previous page)

$$
\begin{aligned}
\frac{d\mathbf{T}^{(4)}}{dt} &= \frac{\dot{m}_{TST}C_{p,4}(\mathbf{T}^{(3)}-\mathbf{T}^{(4)})+\dot{m}_{HP}C_{p,4}(\mathbf{T}^{(7)}-\mathbf{T}^{(4)})}{M_4C_{p,4}} \\
&- \frac{\dot{m}_{HWD}C_{p,4}(\mathbf{T}^{(4)}-\mathbf{T}^{(5)})+U_4A_4(\mathbf{T}^{(4)}-T_{amb})}{M_4C_{p,4}} \\
\frac{d\mathbf{T}^{(5)}}{dt} &= \frac{(\dot{m}_{TST}+\dot{m}_{HP})C_{p,5}(\mathbf{T}^{(4)}-\mathbf{T}^{(5)})-\dot{m}_{HWD}C_{p,5}(\mathbf{T}^{(5)}-\mathbf{T}^{(6)})}{M_5C_{p,5}} \\
&- \frac{U_5A_5(\mathbf{T}^{(5)}-T_{amb})}{M_5C_{p,5}} \\
\frac{d\mathbf{T}^{(6)}}{dt} &= \frac{(\dot{m}_{TST}+\dot{m}_{HP})C_{p,6}(\mathbf{T}^{(5)}-\mathbf{T}^{(6)})-\dot{m}_{HWD}C_{p,6}(\mathbf{T}^{(6)}-T_{tap})}{M_6C_{p,6}} \\
&- \frac{U_6A_6(\mathbf{T}^{(6)}-T_{amb})}{M_6C_{p,6}} \\
\frac{d\mathbf{T}^{(7)}}{dt} &= \frac{\dot{Q}_{HP}+\dot{m}_{HP}C_{p,7}(\mathbf{T}^{(6)}-\mathbf{T}^{(7)})}{M_7C_{p,7}}.
\end{aligned}
$$

Entering the values used in the simulation in Chapter 6 then gives:

$$
\begin{aligned}
\frac{d\mathbf{T}^{(1)}}{dt} &= 0.5256\dot{Q}_{STC}+0.1156(\mathbf{T}^{(2)}-\mathbf{T}^{(1)}) \\
\frac{d\mathbf{T}^{(2)}}{dt} &= 0.1156(\mathbf{T}^{(1)}-\mathbf{T}^{(2)})-1.177*10^{-2}(\mathbf{T}^{(2)}-\mathbf{T}^{(3)}) \\
\frac{d\mathbf{T}^{(3)}}{dt} &= 1.099*10^{-2}(\mathbf{T}^{(6)}-\mathbf{T}^{(3)})+5.878*10^{-4}(\mathbf{T}^{(2)}-\mathbf{T}^{(3)}) \\
&-1.992*10^{-3}\mathbf{T}^{(3)}+0.5840 \\
\frac{d\mathbf{T}^{(4)}}{dt} &= 1.543*10^{-3}(\mathbf{T}^{(3)}-\mathbf{T}^{(4)}+\mathbf{T}^{(7)}-\mathbf{T}^{(4)}) \\
&-1.543*10^{-2}\dot{m}_{HWD}(\mathbf{T}^{(4)}-\mathbf{T}^{(5)}) \\
&-4.792*10^{-6}\mathbf{T}^{(4)}+1.404*10^{-3} \\
\frac{d\mathbf{T}^{(5)}}{dt} &= 3.087*10^{-3}(\mathbf{T}^{(4)}-\mathbf{T}^{(5)})-1.543*10^{-2}\dot{m}_{HWD}(\mathbf{T}^{(5)}-\mathbf{T}^{(6)}) \\
&-4.792*10^{-6}\mathbf{T}^{(5)}+1.404*10^{-3}
\end{aligned}
$$

(continued on next page)

(continued from previous page)

$$\frac{d\mathbf{T}^{(6)}}{dt} = 3.087 * 10^{-3}(\mathbf{T}^{(5)} - \mathbf{T}^{(6)}) - 1.543 * 10^{-2}\dot{m}_{HWD}(\mathbf{T}^{(6)} - 288.15) - 4.792 * 10^{-6}\mathbf{T}^{(6)} + 1.404 * 10^{-3}$$

$$\frac{d\mathbf{T}^{(7)}}{dt} = 2.624 * 10^{-2}\dot{Q}_{HP} + 1.099 * 10^{-2}(\mathbf{T}^{(6)} - \mathbf{T}^{(7)}).$$